

# **The Critical Role of Volatile Organic Compounds Emission in Nitrate Formation in Lhasa, Tibetan Plateau: Insights from Oxygen Isotope Anomaly Measurements**

Xueqin Zheng<sup>a</sup>, Junwen Liu<sup>a\*</sup>, Nima Chuduo<sup>b</sup>, Bian Ba<sup>b</sup>, Pengfei Yu<sup>a</sup>, Phu Drolgar<sup>b</sup>, Fang Cao<sup>c</sup>,  
Yanlin Zhang<sup>c</sup>

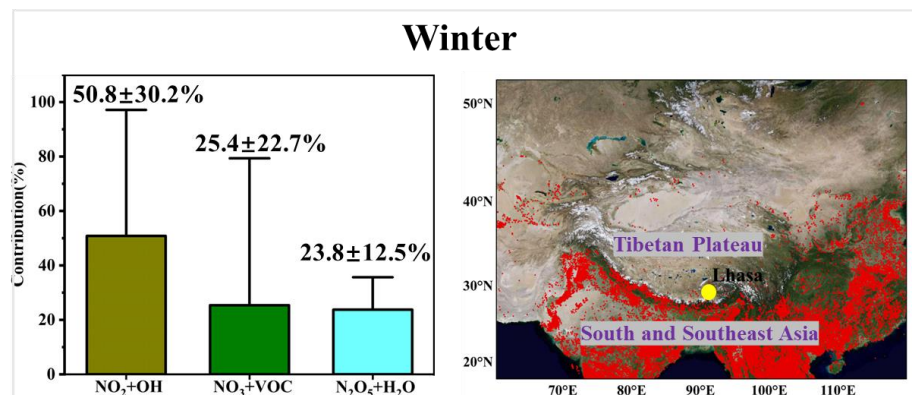
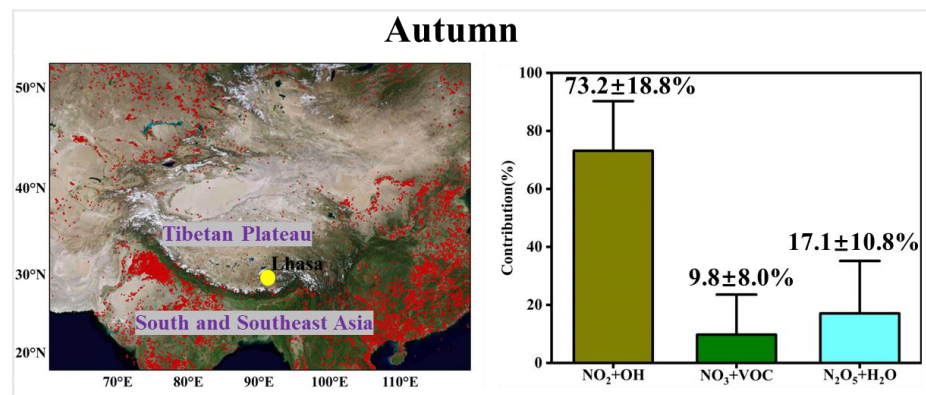
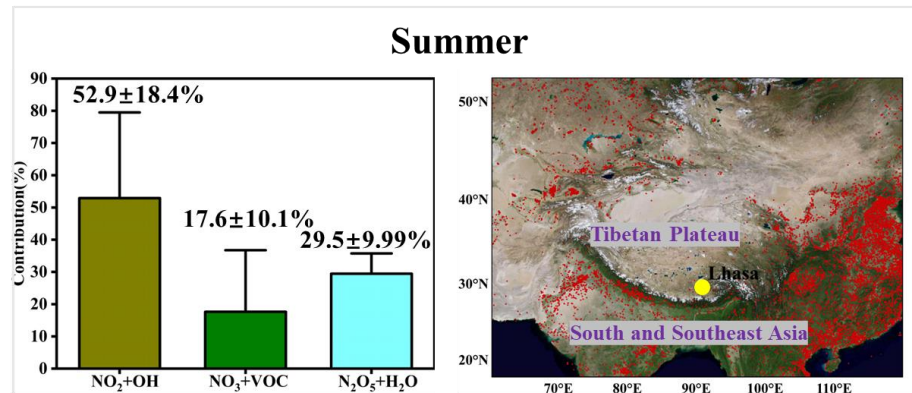
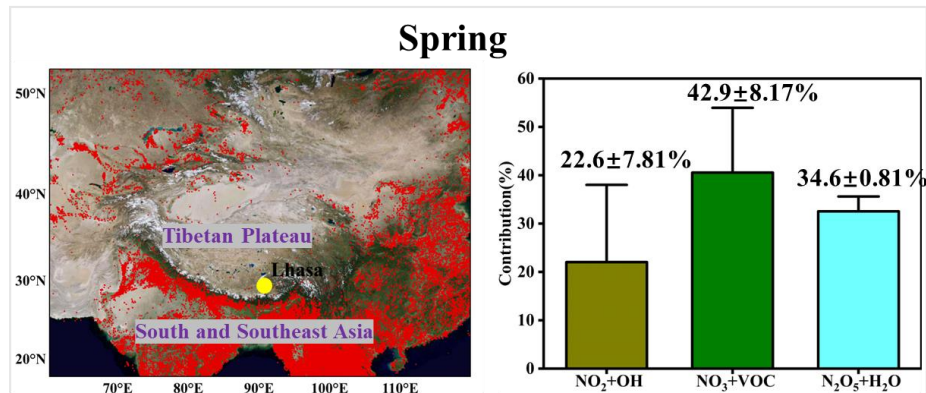
<sup>a</sup> College of Environment and Climate, Jinan University, Guangzhou, 511443, China

<sup>b</sup> Lhasa Meteorological Administration, Lhasa, 850010, China

<sup>c</sup> School of Ecology and Applied Meteorology, Nanjing University of Information Science and Technology, Nanjing 210044, China

\* Corresponding author: Junwen Liu

Email: [liu.junwen@jnu.edu.cn](mailto:liu.junwen@jnu.edu.cn)



TOC art

## Abstract

Atmospheric particulate nitrate aerosol ( $\text{NO}_3^-$ ), produced via the oxidation of nitrogen oxides ( $\text{NO}_x = \text{NO} + \text{NO}_2$ ), plays an important role in atmospheric chemistry and air quality, yet its formation mechanism remains poorly constrained in the plateau region. In this study, we reported for the first time the yearly variation in the signatures of the stable oxygen isotope anomaly ( $\Delta^{17}\text{O} = \delta^{17}\text{O} - 0.52 \times \delta^{18}\text{O}$ ) in  $\text{NO}_3^-$  collected in the urban Lhasa (3650 m a.s.l), on the Tibetan Plateau, China. Our results show that  $\text{NO}_2 + \text{OH}$  was the largest contributor to  $\text{NO}_3^-$  formation ( $46 \pm 26\%$ ), followed by  $\text{NO}_3 + \text{VOC}$  ( $26 \pm 18\%$ ), and  $\text{N}_2\text{O}_5 + \text{H}_2\text{O}$  ( $28 \pm 11\%$ ) using the Bayesian Isotope Mixture Model. Notably, there were significant differences in the  $\text{NO}_2 + \text{OH}$ ,  $\text{NO}_3 + \text{VOC}$ , and  $\text{N}_2\text{O}_5 + \text{H}_2\text{O}$  pathways between spring and the other three seasons (T test,  $p < 0.05$ ). By Hybrid Single-Particle Lagrangian Integrated Trajectory (HYSPLIT) dispersion model, we highlighted the influence of VOC emissions from regions such as Afghanistan and northern India, which enhanced  $\text{NO}_3^-$  concentrations in Lhasa during spring. Furthermore, the diurnal distribution of  $\text{NO}_3^-$  oxidation pathways varied distinctly across seasons, suggesting that these differences in  $\text{NO}_3^-$  pathways are attributed to aerosol liquid water content (ALWC), volatile organic compounds (VOC) concentrations, and atmospheric lifetime of  $\text{NO}_3^-$ .

**Keywords:** nitrate,  $\Delta^{17}\text{O}\text{-NO}_3^-$ , oxidation pathways, Lhasa, VOC

## 1. Introduction

Nitrate aerosol ( $\text{NO}_3^-$ ) is a key component regulating the mass concentration of atmospheric fine particulate matter ( $\text{PM}_{2.5}$ ), which is highly related with air quality (Colmer et al., 2020), public health (Zhang et al., 2019; Zhang et al., 2017; Geng et al., 2021), and climate system (Clark and Tilman, 2008). Globally, the mass contribution of  $\text{NO}_3^-$  in  $\text{PM}_{2.5}$  is in the range of 5-30% (Huang et al., 2014; Xu et al., 2019; Salameh et al., 2015; Espina-Martin et al., 2024; Bell et al., 2007; Sun et al., 2022), depending on the locations and the severities of air pollution. For example, it was reported that  $\text{NO}_3^-$  accounts for 22%, 27% and 26% of  $\text{PM}_{2.5}$  in megacities in China (Zong et al., 2020), Europe (Espina-Martin et al., 2024) and U.S. (Sun et al., 2022), respectively. In addition, some studies found that the contribution of  $\text{NO}_3^-$  would increase by 3-8 times with the occurrence of the particular-derived haze pollution (Ge et al., 2024; Song et al., 2019; Yin et al., 2022; Walters et al., 2024).

It is well-known that atmospheric  $\text{NO}_3^-$  is formed by the oxidation of nitrogen oxides ( $\text{NO}_x = \text{NO} + \text{NO}_2$ ) with different oxidants such as  $\text{O}_3$ ,  $\text{OH}$  and  $\text{RO}_2$  (Text S1). In general, atmospheric chemical transportation models are employed to depict the detailed oxidation pathways of  $\text{NO}_3^-$  formation. However, there remains considerable uncertainty in modelling the contribution of individual oxidation pathways to  $\text{NO}_3^-$  formation, particularly the  $\text{N}_2\text{O}_5 + \text{H}_2\text{O}$  pathway, due to the wide variability of key parameters such as the  $\text{N}_2\text{O}_5$  uptake coefficient, which has been shown to vary significantly depending on aerosol composition, relative humidity, and temperature. For example, it was reported that the predicted  $\text{N}_2\text{O}_5$  uptake to  $\text{NO}_3^-$  formation in Beijing, as estimated using WRF-Chem, ranges from 5% to 21% (Su et al., 2017). Higher contributions between 66% and 85% have been observed when applying the CMAQ model in Beijing (Qiu et al., 2019). Therefore, the application of alternative techniques is crucial for providing more reliable estimates and enhancing our understanding of  $\text{NO}_3^-$  formation mechanisms, in addition to the insights gained from atmospheric chemical transportation models.

Stable oxygen isotope anomaly ( $\Delta^{17}\text{O} = \delta^{17}\text{O} - 0.52 \times \delta^{18}\text{O}$ ) is recognized as a powerful tool to track formation pathways of atmospheric  $\text{NO}_3^-$  (Zhang et al., 2024; Feng et al., 2023). This is because the oxygen atoms in the terminal positions of  $\text{O}_3$  exhibit an elevated  $\Delta^{17}\text{O}$  ( $\Delta^{17}\text{O} = 39 \pm 2\text{‰}$ ) (Vicars and Savarino, 2014), whereas the  $\Delta^{17}\text{O}$  values of other atmospheric oxidants (e.g.,  $\text{H}_2\text{O}$ ,  $\text{OH}$ , and  $\text{RO}_2$ ) that can be incorporated to  $\text{NO}_3^-$  are very close to 0‰. (Dubey et al., 1997; Barkan and Luz, 2003;

Alexander et al., 2020) Therefore,  $\Delta^{17}\text{O}(\text{NO}_3^-)$  serves as a unique tracer of  $\text{O}_3$  involvement in its formation pathways, offering valuable insights into the relative contributions of individual reactions. In recent years, the use of  $\Delta^{17}\text{O}(\text{NO}_3^-)$  to elucidate  $\text{NO}_3^-$  formation has garnered considerable attention. Walters et al. (2024) reported that the major formation pathways of annual  $\text{HNO}_3$  production in the northeastern U.S. were  $\text{NO}_2+\text{OH}$  (46%),  $\text{N}_2\text{O}_5$  uptake (34%), and organic nitrate hydrolysis (12%), with notable seasonal variability. Additionally, Zhang et al. (2022) observed that the contribution of nocturnal chemistry to  $\text{NO}_3^-$  formation increased at night, peaking at 72% around midnight. In contrast, the contribution of  $\text{NO}_2+\text{OH}$  rose with sunrise, reaching its highest fraction (48%) around noon. However, nearly all current  $\Delta^{17}\text{O}$ -related observations have been conducted in the plain cities, with little attention given to plateau cities, where atmospheric conditions generally suffer from distinct energy consumption patterns and unique climatic factors (e.g., intense solar radiation). In this study, we present detailed results from comprehensive field observations conducted in Lhasa (3650 m a.s.l), one of the highest cities in the world, located on the Tibetan Plateau, China. For the first time, we quantify the relative contribution of three oxidation pathways to  $\text{NO}_3^-$  formation in Lhasa on the basis of ambient measurements for  $\Delta^{17}\text{O}$  signatures in  $\text{NO}_3^-$ .

## 2. Materials and methods

### 2.1 Sampling campaign

$\text{PM}_{2.5}$  samples were collected on the roof of a building (~15 m above ground) at the Meteorological Bureau of Lhasa (91.08°E, 29.40°N; Figure 1) in China. Lhasa, the capital of the Tibet Autonomous Region, is a rapidly developing city with a population of ~ 950000 and an urban area of ~ 30000  $\text{km}^2$  (Lhasa). The sampling site is surrounded by mixed land use, including residential areas, government offices, religious temples and commercial zones, with minimal heavy industry. The strong solar radiation and large diurnal temperature variations in this sampling site can lead to pronounced changes in boundary layer height, which in turn significantly influence vertical mixing and the transport of air pollutants.

The sampling campaign was conducted from June 2022 to July 2023 using a high-volume  $\text{PM}_{2.5}$  sampler, which operated at a flow rate of 1.0  $\text{m}^3/\text{min}$ . Samples were collected once a week, with each sampling session lasting 48 hours, except during intensive sampling periods in the summer (June 30

to July 14, 2022) and winter (January 28 to February 7, 2023). During these intensive periods, each sample was collected for 12 hours, from 8:00 to 20:00 and 20:00 to 8:00 on the following day, respectively. During the autumn of 2022, Lhasa experienced intermittent COVID-19 control measures, including restricted movement, reduced traffic activity, and temporary lockdowns in urban areas (Daily). Before sampling, all quartz filters (8 in. × 10 in., Pallflex) were calcined in a muffle furnace at 450 °C for 6 h to prevent impurities from contaminating the collected PM<sub>2.5</sub> samples. After sampling, the samples were collected and stored in a freezer at -20°C.

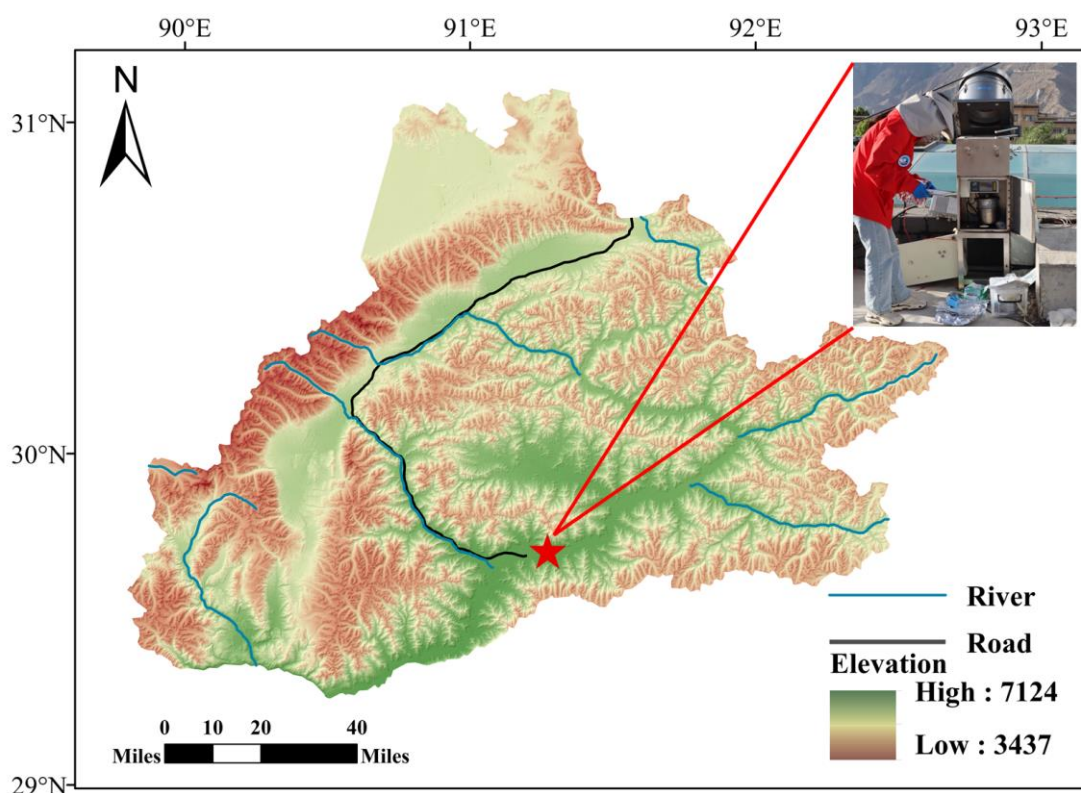


Figure 1. Geographic position of sampling site in Lhasa, China.

## 2.2 Measurements of water-soluble ions and isotopes

Water-soluble ions were measured by an ion chromatography (Dionex ICS-5000, Thermo Scientific Inc.) (Chen et al., 2022). In brief, a part of filter membranes (4.54 cm<sup>2</sup>) was cut using a 17 mm diameter punch and placed in a 15 mL centrifuge tube with 10 mL of 18.2 MΩ ultrapure water. The tube was then subjected to ultrasonic treatment in an ice-water bath for 30 min to prevent ion volatilization. The extract was filtered through a 0.22 μm filter into a 30 mL sample bottle. This process was repeated with an additional 10 mL of water to ensure full extraction. The final extract was analyzed by an ion chromatography. The method detection limits (MDLs) for Cl<sup>-</sup>, NO<sub>3</sub><sup>-</sup>, SO<sub>4</sub><sup>2-</sup>, Na<sup>+</sup>, NH<sub>4</sub><sup>+</sup>, K<sup>+</sup>,

Mg<sup>2+</sup>, and Ca<sup>2+</sup> were 0.001 mg/L, 0.001 mg/L, 0.003 mg/L, 0.02 mg/L, 0.01 mg/L, 0.02 mg/L, 0.006 mg/L, and 0.02 mg/L, respectively.

Stable oxygen isotopes ( $\delta^{17}\text{O}$ ,  $\delta^{18}\text{O}$ ,  $\Delta^{17}\text{O}$ , and  $\Delta^{17}\text{O} = \delta^{17}\text{O} - 0.52 \times \delta^{18}\text{O}$ ) of  $\text{NO}_3^-$  were determined using an isotope ratio mass spectrometer (MAT253, Thermo Fisher Scientific, USA) at Nanjing University of Information Science and Technology (Fan et al., 2021; Zhang et al., 2022). Briefly,  $\text{NO}_3^-$  from filter extractions (containing at least 0.8  $\mu\text{g N}$ ) were converted into gaseous  $\text{N}_2\text{O}$  using the bacterial denitrifier method.  $\text{N}_2\text{O}$  was then further thermally decomposed into  $\text{O}_2$  and  $\text{N}_2$  in a gold tube heated to 800°C. The produced  $\text{O}_2$  was analyzed for oxygen isotopes by isotope ratio mass spectrometer. The duplicated analysis showed that the errors were within 1.32% for  $\Delta^{17}\text{O}-\text{NO}_3^-$ .

### 2.3 Primary data sources

Meteorological parameters, including ambient temperature (T), relative humidity (RH), rainfall, radiation, wind direction (WD) and wind speed (WS) during the sampling campaign, were obtained from the Meteorological Bureau of Lhasa. Additionally,  $\text{NO}_2$  and  $\text{O}_3$  during the sampling campaign were downloaded from the National Meteorological Information Center (<https://air.cnemc.cn:18007/>).

### 2.4 Evaluation of $\text{NO}_3^-$ oxidation pathways

In our study, we aimed to quantify the relative contribution of different oxidation pathways to  $\text{NO}_3^-$  production based on  $\Delta^{17}\text{O}-\text{NO}_3^-$ . Due to the low  $\text{Cl}^-$  concentrations observed in Lhasa, the  $\text{NO}_3^-$  formation pathways considered in this study are limited to  $\text{NO}_2 + \text{OH}$ ,  $\text{NO}_3 + \text{VOC}$ , and  $\text{N}_2\text{O}_5 + \text{H}_2\text{O}$ . Although  $\text{NO}_3 + \text{VOC}$  was generally considered a minor pathway in continental regions (Alexander et al., 2009), we included it because elevated VOC concentrations were observed at our sampling site in Lhasa, influenced by both biogenic emissions (e.g. incense burning) and anthropogenic sources (e.g. vehicle emissions) (Tang et al., 2022). The relative contributions of the three pathways were determined using a  $\Delta^{17}\text{O}$ -based mass balance approach (Michalski et al., 2003), as shown in Equations (1) and (2):

$$\Delta^{17}\text{O}-\text{NO}_3^- = (\Delta^{17}\text{O}-\text{NO}_3^-)_{\text{NO}_2+\text{OH}} \times f_{\text{NO}_2+\text{OH}} + (\Delta^{17}\text{O}-\text{NO}_3^-)_{\text{NO}_3+\text{VOC}} \times f_{\text{NO}_3+\text{VOC}} + (\Delta^{17}\text{O}-\text{NO}_3^-)_{\text{N}_2\text{O}_5+\text{H}_2\text{O}} \times f_{\text{N}_2\text{O}_5+\text{H}_2\text{O}} \quad (1)$$

$$f_{\text{NO}_2+\text{OH}} + f_{\text{NO}_3+\text{VOC}} + f_{\text{N}_2\text{O}_5+\text{H}_2\text{O}} = 1 \quad (2)$$

where  $\Delta^{17}\text{O}-\text{NO}_3^-$  value is the  $\Delta^{17}\text{O}$  value of  $\text{NO}_3^-$  in  $\text{PM}_{2.5}$ . The  $(\Delta^{17}\text{O}-\text{NO}_3^-)_{\text{NO}_2+\text{OH}}$ ,  $(\Delta^{17}\text{O}-\text{NO}_3^-)_{\text{NO}_3+\text{VOC}}$ , and  $(\Delta^{17}\text{O}-\text{NO}_3^-)_{\text{N}_2\text{O}_5+\text{H}_2\text{O}}$  correspond to the  $\Delta^{17}\text{O}$  values from  $\text{NO}_2+\text{OH}$ ,  $\text{NO}_3+\text{VOC}$  and

$\text{N}_2\text{O}_5 + \text{H}_2\text{O}$ , respectively. The  $\Delta^{17}\text{O}$  values for each pathway were calculated using Equations (3), (4), and (5) (Savarino et al., 2016; Alexander et al., 2009):

$$(\Delta^{17}\text{O}-\text{NO}_3^-)_{\text{NO}_2+\text{OH}} (\text{‰}) = 2/3\alpha \times \Delta^{17}\text{O}-\text{O}_3^* \quad (3)$$

$$(\Delta^{17}\text{O}-\text{NO}_3^-)_{\text{NO}_3+\text{VOC}} (\text{‰}) = 2/3\alpha \times \Delta^{17}\text{O}-\text{O}_3^* + 1/3 \times \Delta^{17}\text{O}-\text{O}_3^* \quad (4)$$

$$(\Delta^{17}\text{O}-\text{NO}_3^-)_{\text{N}_2\text{O}_5+\text{H}_2\text{O}} (\text{‰}) = 1/3\alpha \times \Delta^{17}\text{O}-\text{O}_3^* + 1/2(2/3\alpha \times \Delta^{17}\text{O}-\text{O}_3^* + 1/3 \times \Delta^{17}\text{O}-\text{O}_3^*) \quad (5)$$

Previous studies have demonstrated a linear correlation between  $\Delta^{17}\text{O}-\text{O}_3$  and  $\Delta^{17}\text{O}-\text{O}_3^*$ , with  $\Delta^{17}\text{O}(\text{O}_3)$  values ranging from 20‰ to 40‰ in tropospheric  $\text{O}_3$  (Vicars and Savarino, 2014; Ishino et al., 2017).

The equations are shown as follows (Vicars et al., 2012):

$$\Delta^{17}\text{O}-\text{O}_3^* = 1.5 \times \Delta^{17}\text{O}-\text{O}_3 \quad (6)$$

Based on previous observations of tropospheric  $\text{O}_3$ ,  $\Delta^{17}\text{O}-\text{O}_3^*$  average value was approximately 39‰.

The  $\alpha$  value represents the proportional contribution of  $\text{O}_3$  to the  $\text{NO}$  oxidation pathway and can be estimated using the following equations (7) (Alexander et al., 2009). When  $\text{NO}_x$  is in photochemical steady state,  $\Delta^{17}\text{O}-\text{NO}_2$  can be represented using the following equation (10):

$$\alpha = K_{P1} [\text{O}_3] \times [\text{NO}] / (K_{P1} \times [\text{O}_3] \times [\text{NO}] + K_{P2} \times [\text{NO}] \times [\text{HO}_2] + K_{P3} \times [\text{NO}] \times [\text{RO}_2]) \quad (7)$$

$$K_{P1} = 3.0 \times 10^{-12} \times e^{(-1500/T)} \quad (8)$$

$$K_{P2} = K_{P3} = 3.5 \times 10^{-12} \times e^{(270/T)} (\text{cm}^3 \cdot \text{molecule}^{-1} \cdot \text{s}^{-1}) \quad (9)$$

$$\Delta^{17}\text{O}-\text{NO}_2 = \alpha \Delta^{17}\text{O}-\text{O}_3^* \quad (10)$$

where  $T$  represents the ambient temperature (K) (Kunasek et al., 2008). The  $\text{HO}_2$  mixing ratios were estimated using empirical equations in the absence of direct  $\text{HO}_2$  observations (Kanaya et al., 2007). Due to the lower temperatures in Lhasa during non-summer seasons,  $\text{HO}_2$  concentrations were assessed using a formula derived from winter conditions.

Winter

$$[\text{HO}_2 \cdot] / \text{ppt} = \exp(5.7747 \times 10^{-2} [\text{O}_3] (\text{ppb}) - 1.7227) \text{ for daytime} \quad (11)$$

$$[\text{HO}_2 \cdot] / \text{ppt} = \exp(7.7234 \times 10^{-2} [\text{O}_3] (\text{ppb}) - 1.6363) \text{ for nighttime} \quad (12)$$

Summer

$$[\text{HO}_2 \cdot] / \text{pptv} = \exp(2.0706 \times 10^{-2} [\text{O}_3] (\text{ppb}) + 1.0625) \text{ for daytime} \quad (13)$$

$$[\text{HO}_2 \cdot] / \text{pptv} = 0.2456 + 0.1841 [\text{O}_3] (\text{ppb}) \text{ for nighttime} \quad (14)$$

## 2.5 Stable isotope analysis in the R (SIAR) model

In this study, stable isotope analysis in the R (SIAR) model was employed to estimate the relative contributions of three main pathways to  $\text{NO}_3^-$  (Parnell et al., 2010). The SIAR model is well-suited for



analyzing multiple formation pathways, as it effectively incorporates uncertainties and parameter variability, leading to more reliable estimates. Specifically, this model allows for a detailed analysis of oxygen isotope ( $\Delta^{17}\text{O}$ ), enabling accurate modeling of  $\text{NO}_3^-$  formation pathways based on oxygen isotope measurements. The SIAR model is a Bayesian mixture model, mathematically formulated as follows:

$$X_i = \sum_{j=1}^K p_j \times f_{ij}$$

$$p_1 + p_2 + \dots + p_k = 1$$

$$f_{ij} \sim N(\mu_j, \omega_j^2)$$

Where  $X_i$  is the observed  $\Delta^{17}\text{O}$  values for sample  $i$  ( $i = 1, 2, 3, \dots, N$ ) and  $p_j$  is the proportional contribution of each  $\text{NO}_3^-$  formation pathway  $j$  to the sample  $i$ .  $f_{ij}$  is the  $\Delta^{17}\text{O}$  values of formation pathway  $j$  for sample  $i$  and follows a normal distribution with mean ( $\mu_j$ ) and variance ( $\omega_j^2$ ). Within the Bayesian framework, prior distributions are assigned to each  $p_j$ , and these are updated with the observed data  $X_i$  to obtain posterior distributions, allowing for inference of the proportional contributions  $p_j$  of each pathway.

## **2.6 Aerosol liquid water content (ALWC) and the Hybrid Single-Particle Lagrangian Integrated Trajectory (HYSPLIT)**

To evaluate the influence of ALWC on the  $\text{NO}_3^-$  formation, ALWC was calculated using the ISORROPIA II model developed by Fountoukis and Nenes (Fountoukis and Nenes, 2007). The ISORROPIA II model includes two modes: the forward mode, which requires the concentrations of both particulate and gaseous pollutants concentrations as inputs, and the reverse mode, which only requires the concentrations of particulate pollutants concentrations. The model computes the ALWC in both modes based on particulate pollutant concentrations (e.g.,  $\text{NH}_4^+$ ,  $\text{Na}^+$ ,  $\text{Ca}^{2+}$ ,  $\text{K}^+$  and  $\text{Mg}^{2+}$ ), as well as ambient RH and T. In this study, the reverse mode was employed due to the lack of gaseous pollutant concentrations observations.

Additionally, the Hybrid Single-Particle Lagrangian Integrated Trajectory (HYSPLIT) model was utilized to compute 72-hour back trajectories during the sampling campaign. HYSPLIT, developed by the National Oceanic and Atmospheric Administration Air Resources Laboratory (NOAA/ARL), is available on their website (<https://www.ready.noaa.gov/HYSPLIT.php>). This model has been widely

used for simulating the transport and dispersion trajectories of pollutants such as PM<sub>2.5</sub>, VOC, O<sub>3</sub>, and NO<sub>x</sub>, among others (He et al., 2022; Zhao et al., 2015; Cao et al., 2023). Backward trajectories for each sampling day were calculated at an altitude of 3650 meters using meteorological data from the Global Data Assimilation System (GDAS), available through the US Air Resources Laboratory (NOAA ARL) (<https://www.ready.noaa.gov/data/archives/gdas1/>).

### 3. Results

#### 3.1 Overview of the meteorological parameters in Lhasa during the sampling campaign

Figure 2a presents the daily variations in meteorological parameters, including temperature, relative humidity (RH), rainfall and solar radiation. During the sampling campaign, the annual average temperature was 11.5°C, ranging from -2.83 to 24.2°C. The highest average temperature was observed in summer (19.7°C), while the lowest (3.11°C) was recorded in winter. Relative humidity (RH) varied between 6.67 and 66.8%, with the lowest average RH occurring in winter (17.1%) and the highest in summer (35.6%). The near-surface layer of Lhasa is influenced by a thermal low-pressure system, and the southwest monsoon, active between June and September, transports moisture-laden air from the Indian Ocean, resulting in increased rainfall during summer. Solar radiation intensity exhibited a seasonal trend consistent to those of temperature and RH, peaking in summer (394 W/m<sup>2</sup>) and reaching its lowest levels in winter (220 W/m<sup>2</sup>). The dominant wind direction (WD) was southeast in spring, but southwest in the other three seasons (Figure 3). Wind speed (WS) was highest in spring but lowest in autumn.

#### 3.2 NO<sub>3</sub><sup>-</sup> concentration

NO<sub>3</sub><sup>-</sup> mass concentrations ranged from 0.10 to 1.72 µg/m<sup>3</sup>, with an average value of 0.62 ± 0.31 µg/m<sup>3</sup>. NO<sub>3</sub><sup>-</sup> concentrations exhibited distinct seasonal patterns. As shown in Figure S1, the equivalent concentrations of [SO<sub>4</sub><sup>2-</sup> + NO<sub>3</sub><sup>-</sup>] were considerably higher than those of [NH<sub>4</sub><sup>+</sup>], indicating that NH<sub>4</sub><sup>+</sup> was insufficient to fully neutralize NO<sub>3</sub><sup>-</sup>. This suggests that a portion of NO<sub>3</sub><sup>-</sup> may have existed in other forms, such as KNO<sub>3</sub> and Ca(NO<sub>3</sub>)<sub>2</sub>. This inference is supported by the strong positive correlations between NO<sub>3</sub><sup>-</sup> and K<sup>+</sup> (r = 0.64, p < 0.1) and Ca<sup>2+</sup> (r = 0.43, p < 0.01), especially in spring, as shown in Figure S2. In contrast, NO<sub>3</sub><sup>-</sup> showed relatively weak negative correlations with T (r = -0.27, p < 0.01) and RH (r = -0.22, p < 0.1), indicating that under the specific atmospheric conditions in Lhasa,

meteorological parameters might not be the dominant factors controlling the gas-particle partitioning of  $\text{NO}_3^-$ . The maximum monthly average values of  $\text{NO}_3^-$  concentration occurred in spring ( $0.83 \pm 0.35 \mu\text{g}/\text{m}^3$ ) with the instantaneous maximum reaching  $1.72 \mu\text{g}/\text{m}^3$ , whereas the lowest was recorded in autumn ( $0.23 \pm 0.13 \mu\text{g}/\text{m}^3$ ) with an instantaneous minimum of only  $0.09 \mu\text{g}/\text{m}^3$  (Table 1). The elevated  $\text{NO}_3^-$  concentrations in spring could be attributed to biomass burning emitted from south and Southeast Asia (Figure S3/Figure S4). The strong between  $\text{NO}_3^-$  and  $\text{K}^+$  in spring further this explanation.

In spring, high  $\text{NO}_3^-$  concentrations were associated with weak southeasterly winds ( $< 3 \text{ m/s}$ ) in the bivariate polar plot, suggesting probable impacts from local emissions (Figure 3). The southeasterly sector of sampling site includes residential areas, agriculture land and major transportation routes, which are potential  $\text{NO}_x$  sources. In spring, intensified agriculture activities (e.g., fertilization, biomass burning) might increase  $\text{NO}_x$  emissions. Meanwhile, low wind speeds likely limit atmospheric dispersion, promoting the local accumulation of precursors and enhancing  $\text{NO}_3^-$  production. During the rainy summer, shorter  $\text{NO}_3^-$  lifetimes indicated a weak influence from regional transport, with a more pronounced contribution from local emissions. In autumn,  $\text{NO}_3^-$  concentrations were relatively low, which coincided with strict local COVID-19 restrictions in Lhasa. These measures significantly reduced human activity and traffic, leading to suppressed local emissions. Despite low wind speeds typically favor pollutant accumulation,  $\text{NO}_3^-$  concentrations remained low, suggesting that both reduced local sources and seasonal meteorological conditions constrained  $\text{NO}_3^-$  production. Nevertheless, the persistence of measurable  $\text{NO}_3^-$  under such stagnant conditions also implied a potential contribution from regional transport during this period. In winter, elevated  $\text{NO}_3^-$  concentrations under low wind speeds ( $< 3 \text{ m/s}$ ) emphasized the significant contribution of local emissions. These findings underscored that both regional transport and local emissions were important contributors to  $\text{NO}_3^-$  concentrations in Lhasa. Furthermore, based on our day-night sampling scheme, no nycthemeral (day-night) differences in  $\text{NO}_3^-$  concentrations were detected (Table S1). A similar day-night pattern of  $\text{NO}_3^-$  concentrations also has been observed in Beijing (Luo et al., 2020).

266 Table 1 Average values of water-soluble ions and  $\Delta^{17}\text{O-NO}_3^-$  during the sampling campaign

267

		$\text{Na}^+$	$\text{NH}_4^+$	$\text{K}^+$	$\text{Mg}^{2+}$	$\text{Ca}^{2+}$	$\text{Cl}^-$	$\text{NO}_3^-$	$\text{SO}_4^{2-}$	$\Delta^{17}\text{O-NO}_3^-$
		$\mu\text{g/m}^3$	$\mu\text{g/m}^3$	$\mu\text{g/m}^3$	$\mu\text{g/m}^3$	$\mu\text{g/m}^3$	$\mu\text{g/m}^3$	$\mu\text{g/m}^3$	$\mu\text{g/m}^3$	‰
<b>Annual</b>	<b>Minmum</b>	0.02	0	0.004	0.004	0.004	0.004	0.09	0.06	18.3
	<b>Maximum</b>	0.68	1.22	0.29	0.08	3.52	0.51	1.72	2.37	34.1
	<b>Average</b>	0.16	0.3	0.07	0.02	1.09	0.08	0.62	0.74	26.3
	<b>Std.Dev</b>	0.14	0.26	0.06	0.01	0.7	0.1	0.31	0.45	3.13
<b>spring</b>	<b>Minmum</b>	0.04	0.16	0.04	0.01	1.02	0.01	0.45	0.6	27.2
	<b>Maximum</b>	0.16	1.22	0.2	0.05	2.56	0.05	1.72	2.14	30.4
	<b>Average</b>	0.09	0.52	0.09	0.02	1.67	0.03	0.83	1.11	28.8
	<b>Std.Dev</b>	0.03	0.3	0.04	0.01	0.51	0.01	0.35	0.52	0.99
<b>summer</b>	<b>Minmum</b>	0.02	0	0.01	0.01	0.03	0.003	0.13	0.18	20.2
	<b>Maximum</b>	0.4	1.08	0.09	0.04	2.4	0.13	1	2.37	28.5
	<b>Average</b>	0.09	0.18	0.03	0.02	1.15	0.3	0.5	0.72	25.5
	<b>Std.Dev</b>	0.08	0.17	0.02	0.01	0.5	0.3	0.23	0.45	2.2
<b>autumn</b>	<b>Minmum</b>	0.02	0.003	0.004	0.01	0.004	0.01	0.09	0.06	21.2
	<b>Maximum</b>	0.17	0.11	0.1	0.03	0.24	0.17	0.51	0.55	24.9
	<b>Average</b>	0.09	0.04	0.3	0.02	0.13	0.05	0.23	0.31	23.05
	<b>Std.Dev</b>	0.05	0.04	0.3	0.01	0.08	0.05	0.13	0.14	1.44
<b>winter</b>	<b>Minmum</b>	0.06	0.09	0.02	0.01	0.05	0.04	0.21	0.32	18.3
	<b>Maximum</b>	0.56	0.87	0.29	0.08	3.52	0.51	1.46	1.57	34.1
	<b>Average</b>	0.19	0.44	0.12	0.03	1.04	0.16	0.75	0.73	25.9
	<b>Std.Dev</b>	0.12	0.21	0.08	0.02	0.78	0.13	0.28	0.34	3.86

268

269

270

### 3.3 Oxygen isotopes of $\text{NO}_3^-$

To explore the three major oxidation pathways of  $\text{NO}_3^-$  formation, 53 samples representing varying  $\text{NO}_3^-$  concentrations across different seasons were selected for oxygen isotope measurements (Figure 2b). The  $\Delta^{17}\text{O}-\text{NO}_3^-$  values ranged from 18.3 to 34.1‰, with an average of  $26.3 \pm 3.13\text{‰}$ , which is slightly lower than the global average of  $28.6 \pm 4.5\text{‰}$  simulated by the Global Chemical Transport Model (Alexander et al., 2020). As shown in Table S2, the observed  $\Delta^{17}\text{O}-\text{NO}_3^-$  values in this study were similar to most mid- and low-latitude regions, but lower than those in polar regions ( $\sim 32\text{‰}$ ). As listed in Table S1, the average  $\Delta^{17}\text{O}-\text{NO}_3^-$  values in spring, summer, autumn and winter were  $28.8 \pm 8.0\text{‰}$ ,  $25.5 \pm 2.20\text{‰}$ ,  $25.6 \pm 1.35\text{‰}$  and  $25.9 \pm 3.56\text{‰}$ , respectively. The differences in  $\Delta^{17}\text{O}-\text{NO}_3^-$  values between spring and summer, as well as between spring and winter, were statistically significant ( $p < 0.05$ ). The elevated  $\Delta^{17}\text{O}-\text{NO}_3^-$  values in spring could be attributed to a higher proportion of nocturnal pathways that enrich  $\Delta^{17}\text{O}-\text{NO}_3^-$  values, such as  $\text{NO}_3 + \text{VOC}$  and  $\text{N}_2\text{O}_5 + \text{H}_2\text{O}$  pathway. In contrast, the lower  $\Delta^{17}\text{O}-\text{NO}_3^-$  values in other three seasons suggested a greater production of  $\text{NO}_3^-$  formation via  $\text{NO}_2 + \text{OH}$  pathway, leading to more negative  $\Delta^{17}\text{O}-\text{NO}_3^-$  values. Diurnal variation in  $\Delta^{17}\text{O}-\text{NO}_3^-$  values also differed across season (Figure S5). In summer, the average of  $\Delta^{17}\text{O}-\text{NO}_3^-$  values during the day ( $25.3 \pm 2.39\text{‰}$ ) was lower than at night ( $26.7 \pm 1.03\text{‰}$ ). Conversely, in winter, the average of  $\Delta^{17}\text{O}-\text{NO}_3^-$  values during the day ( $28.0 \pm 3.79\text{‰}$ ) was significantly higher than at night ( $24.4 \pm 3.85\text{‰}$ ). Similar diurnal patterns, with higher daytime  $\Delta^{17}\text{O}-\text{NO}_3^-$  values and lower nighttime values, have also been observed in winter in the U.S. (Vicars et al., 2013) and other cities in China (He et al., 2018).

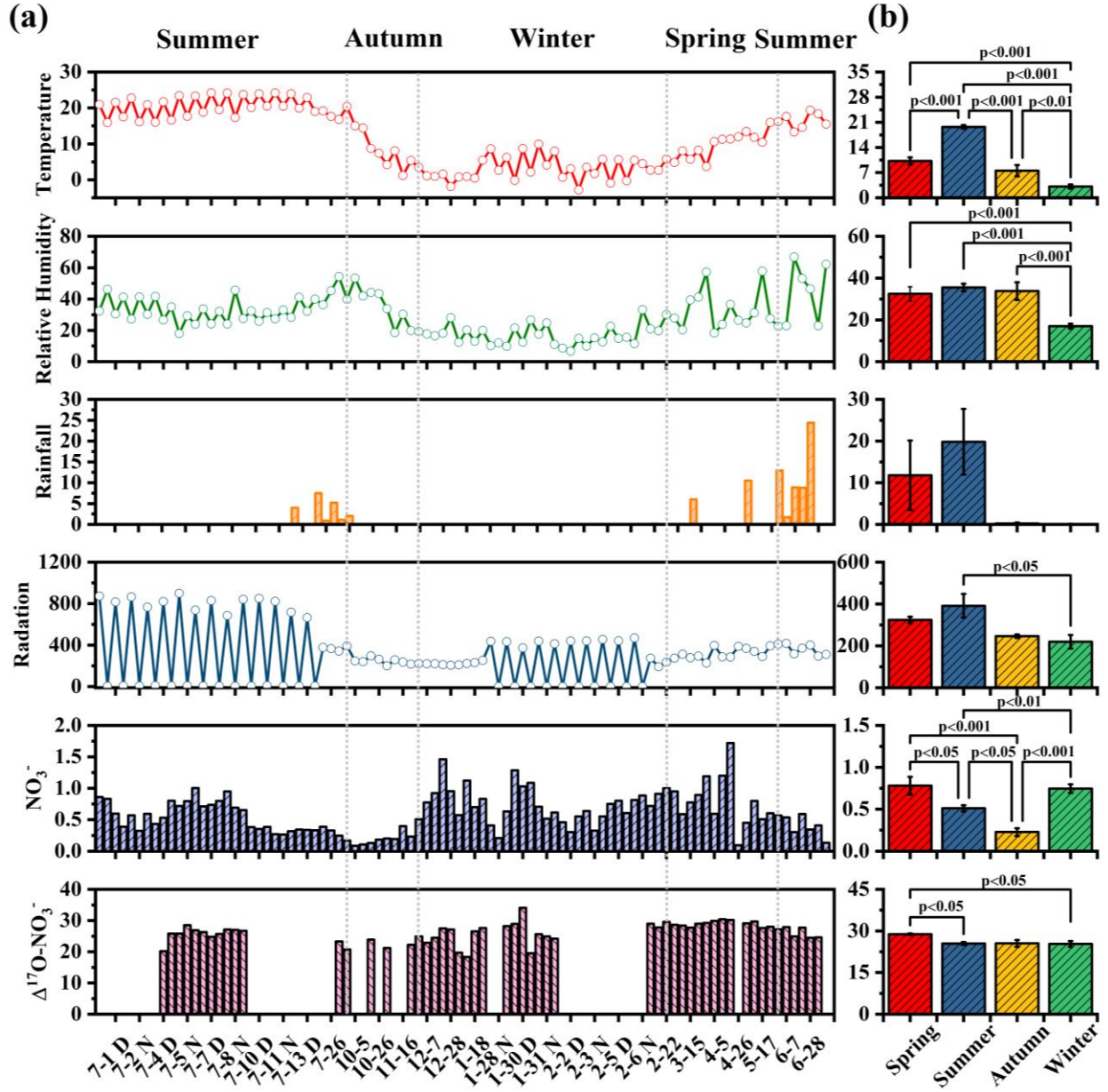
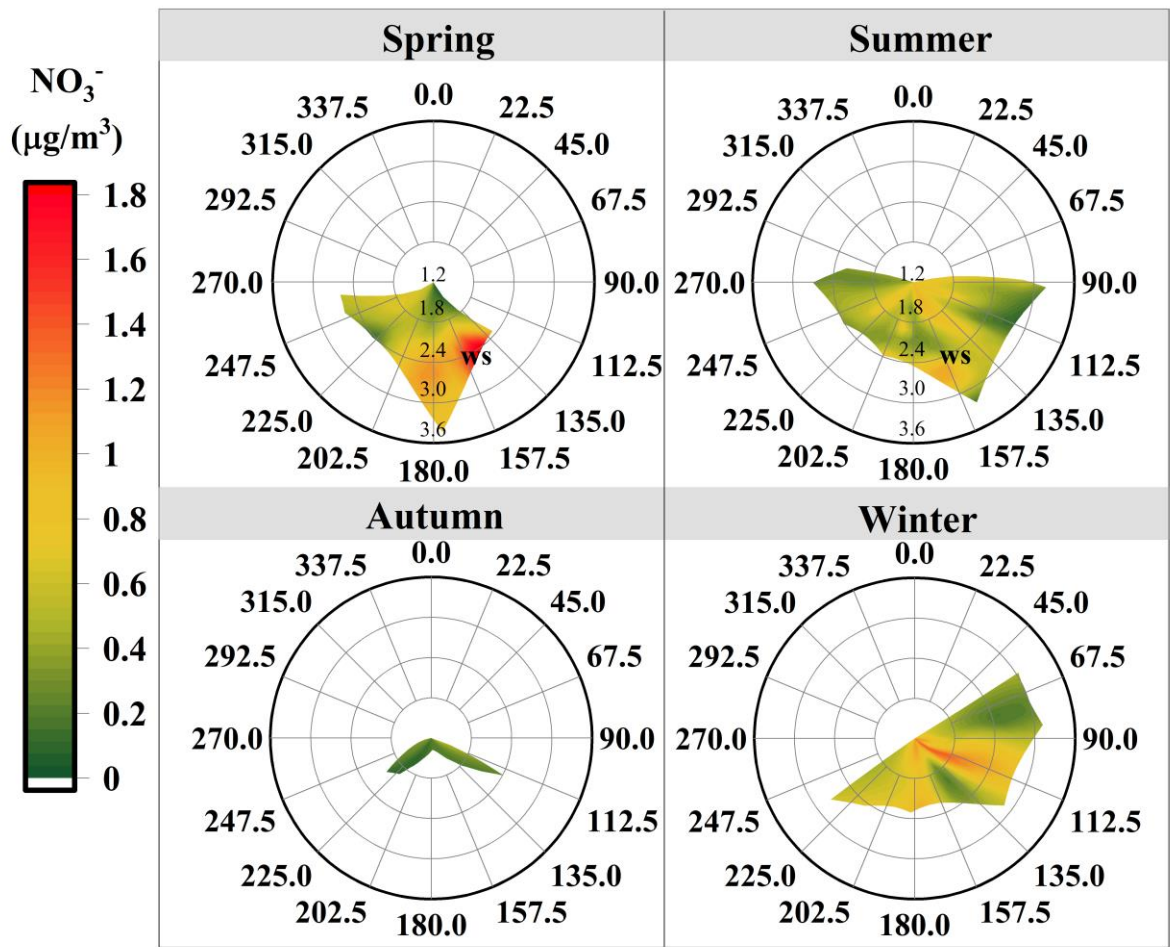


Figure 2. (a) shows the time series of temperature ( $^{\circ}C$ ), relative humidity (%), Rainfall (mm), Radiation ( $W/m^2$ ),  $NO_3^-$  concentration ( $\mu g/m^3$ ), and  $\Delta^{17}O-NO_3^-$  (‰) from June 2022 to July 2023. (b) shows the average values significance at different seasons with their statistical.



298

299 *Figure 3. Bivariate polar plot illustrates the seasonal variation in the mass concentration of  $\text{NO}_3^-$  in*  
300 *relation to wind speed (WS, m/s) and wind direction (WD, degrees).*

301

## 302 4. Discussion

### 303 4.1 A comparison of $\text{NO}_3^-$ oxidation pathways in Lhasa with other megacities in plain regions

304 Typically, observations of  $\Delta^{17}\text{O}-\text{NO}_3^-$  and estimated  $\alpha$  (the proportion of  $\text{O}_3$  oxidation in  $\text{NO}_2$   
305 production rate) values are employed to quantify the contributions of major  $\text{NO}_3^-$  oxidation pathway  
306 in conjunction with a Bayesian model. The  $\alpha$  value ranged from 0.63 to 0.93, with an average of  $0.83$   
307  $\pm 0.06$ , suggesting the significance of  $\text{O}_3$  participation in  $\text{NO}$  oxidation during the sampling campaign.  
308 On the other hand, our  $\alpha$  values were lower than those (0.85-1) for other midlatitude regions  
309 (Alexander et al., 2009). The  $\alpha$  values are influenced by the relative amount of  $\text{O}_3$ ,  $\text{HO}_2$  and  $\text{RO}_2$  in  
310  $\text{NO}_x$  cycling. Due to the generally high  $\text{O}_3$  concentrations ( $\text{O}_3 > 50$  ppb) observed in Lhasa, nearly all

$\alpha$  values exceeded 0.8 (Figure S6). To evaluate the impact of key parameters on the estimated contributions of different  $\text{NO}_3^-$  formation pathways, we conducted a sensitivity analysis by assumed the  $\alpha$  values and  $\Delta^{17}\text{O}$  value of the terminal oxygen atoms of  $\text{O}_3$  ( $\Delta^{17}\text{O}-\text{O}_3^*$ ). As listed in Table S3, the assumption of  $\alpha$  and  $\Delta^{17}\text{O}-\text{O}_3^*$  have an impact on the  $\text{NO}_3^-$  formation mechanisms. When  $\Delta^{17}\text{O}-\text{O}_3^*$  was fixed at 39‰, increasing  $\alpha$  from 0.7 to 0.9 led to a notable increase in the relative contribution of the  $\text{NO}_2 + \text{OH}$  pathway from 25% to 46%, while that of the  $\text{NO}_3 + \text{VOC}$  pathway decreased from 46% to 25%. The  $\text{N}_2\text{O}_5 + \text{H}_2\text{O}$  pathway remained nearly constant, with contributions ranging between 28% and 29%, indicating that this pathway is relatively insensitive to changes in  $\alpha$  values. Similarly, when  $\alpha$  was varied within a reasonable range (0.68-0.93), increasing the  $\Delta^{17}\text{O}-\text{O}_3^*$  value from 37‰ to 39‰ led to an increase in the  $\text{NO}_2 + \text{OH}$  contribution from 37% to 46%, and a corresponding decrease in the  $\text{NO}_3 + \text{VOC}$  contribution from 35% to 26%. Again, the  $\text{N}_2\text{O}_5 + \text{H}_2\text{O}$  contribution remained stable at  $\sim 28\%$ . These results suggest that the estimated contributions of  $\text{NO}_2 + \text{OH}$  and  $\text{NO}_3 + \text{VOC}$  pathways are sensitive to assumptions about  $\alpha$  and  $\Delta^{17}\text{O}-\text{O}_3^*$ , whereas the contribution of the  $\text{N}_2\text{O}_5 + \text{H}_2\text{O}$  pathway is relatively robust under the tested conditions. Because Lhasa is characterized by relatively high VOC concentrations and  $\Delta^{17}\text{O}-\text{O}_3^*$  is generally close to 39‰, we consider our parameter assumptions reasonable for further estimating  $\text{NO}_3^-$  formation pathways for each sample..

On average, the relative contributions of  $\text{NO}_2 + \text{OH}$  ( $f_{\text{NO}_2+\text{OH}}$ ),  $\text{NO}_3 + \text{VOC}$  ( $f_{\text{NO}_3+\text{VOC}}$ ) and  $\text{N}_2\text{O}_5 + \text{H}_2\text{O}$  ( $f_{\text{N}_2\text{O}_5+\text{H}_2\text{O}}$ ) to  $\text{NO}_3^-$  formation in Lhasa during the sampling campaign were  $46 \pm 26\%$ ,  $26 \pm 19\%$  and  $28 \pm 11\%$ , respectively. To better understand the characteristics of  $\text{NO}_3^-$  formation mechanism in Lhasa, we performed a detailed comparison around the China for the relative contributions of key oxidation pathways using the  $\Delta^{17}\text{O}$  methodology (Figure 4). Overall, similar to most Chinese cities,  $\text{NO}_3^-$  formation in Lhasa was predominantly driven by the  $\text{NO}_2 + \text{OH}$  pathway, exhibiting distinct seasonal and regional variations. In particular, the average  $f_{\text{NO}_3+\text{VOC}}$  values were generally several times higher in spring in Lhasa than in other urban cities. Compared to rural/remote areas, the average  $f_{\text{NO}_3+\text{VOC}}$  values showed higher fractions in Lhasa, revealing the influence of anthropogenic emission, i.e., vehicle exhaust and heating, on  $\text{NO}_3^-$  formation. In Lhasa, the Capital of Tibet, field measurements among different years showed a substantial increase in VOC concentrations in urban areas of the Tibet Plateau, comparable to those in North China (Tang et al., 2022), revealing the importance of the active  $\text{NO}_3 + \text{VOC}$  pathway for  $\text{NO}_3^-$  pollution formation in Lhasa. In fact, recent studies have recognized  $\text{NO}_3 + \text{VOC}$  as a major formation mechanism for  $\text{NO}_3^-$  production. For instance, Fan et al. (2021)



found that  $f_{\text{NO}_3+\text{VOC}}$  in Beijing increased from 17% in summer to 32% in winter based on  $\Delta^{17}\text{O}-\text{NO}_3^-$  measurements. He et al. (2018) estimated the relative contributions of  $\text{NO}_3 + \text{VOC}$  and  $\text{N}_2\text{O}_5 + \text{Cl}^-$  to  $\text{NO}_3^-$  formation and found that  $\text{NO}_3 + \text{VOC}$  and  $\text{N}_2\text{O}_5 + \text{Cl}^-$  were in the range of 16-56%, underscoring the significant roles of these pathways during haze events in Beijing. Similarly, Feng et al. (2023) also reported that the  $f_{\text{NO}_3+\text{VOC}}$  values were up to 49.6% in winter in northern China. In Guangzhou, Wang et al. (2023) noted that the average  $f_{\text{NO}_3+\text{VOC}}$  value was at the 488m (25%) higher than that at the ground (12%). Furthermore, Li et al. (2022) reported that  $f_{\text{NO}_3+\text{VOC}}$  increased from 5% in urban to 13.5% in rural regions in Northeast China. Although the specific nighttime  $\text{RO}_2$  production mechanism in Lhasa remains unclear, studies in other cities have demonstrated that  $\text{NO}_3+\text{VOC}$  pathway was the dominant channel for nighttime  $\text{RO}_2$  (Fisher et al., 2016), which in turn leads to the formation of alkyl and multifunctional nitrates ( $\text{RONO}_2$ ) and eventually  $\text{NO}_3^-$ . In such cases, the  $\text{RO}_2$  concentration is expected to be correlated with  $\text{NO}_3$  radical production, which depends on the reaction rate of  $\text{O}_3$  and  $\text{NO}_2$  (Brown and Stutz, 2012). Given the relatively high nighttime  $\text{O}_3$  concentrations in Lhasa, it is plausible that  $\text{O}_3$ -driven nighttime  $\text{NO}_3$  chemistry plays an important role, thereby enhancing  $\text{NO}_3+\text{VOC}$  derived from  $\text{RO}_2$  production and  $\text{NO}_3^-$  formation. Global modelling studies also support the significant of this pathway. For instance, Alexander et al. (2020) reported that the  $\text{NO}_3 + \text{VOC}$  pathway via the  $\text{RONO}_2$  mechanism accounted for 3% of global  $\text{NO}_3^-$  formation on average. The relatively high  $f_{\text{NO}_3+\text{VOC}}$  values observed in Lhasa are broadly consistent with these findings, especially under conditions of high VOC concentrations and strong nighttime oxidant levels.

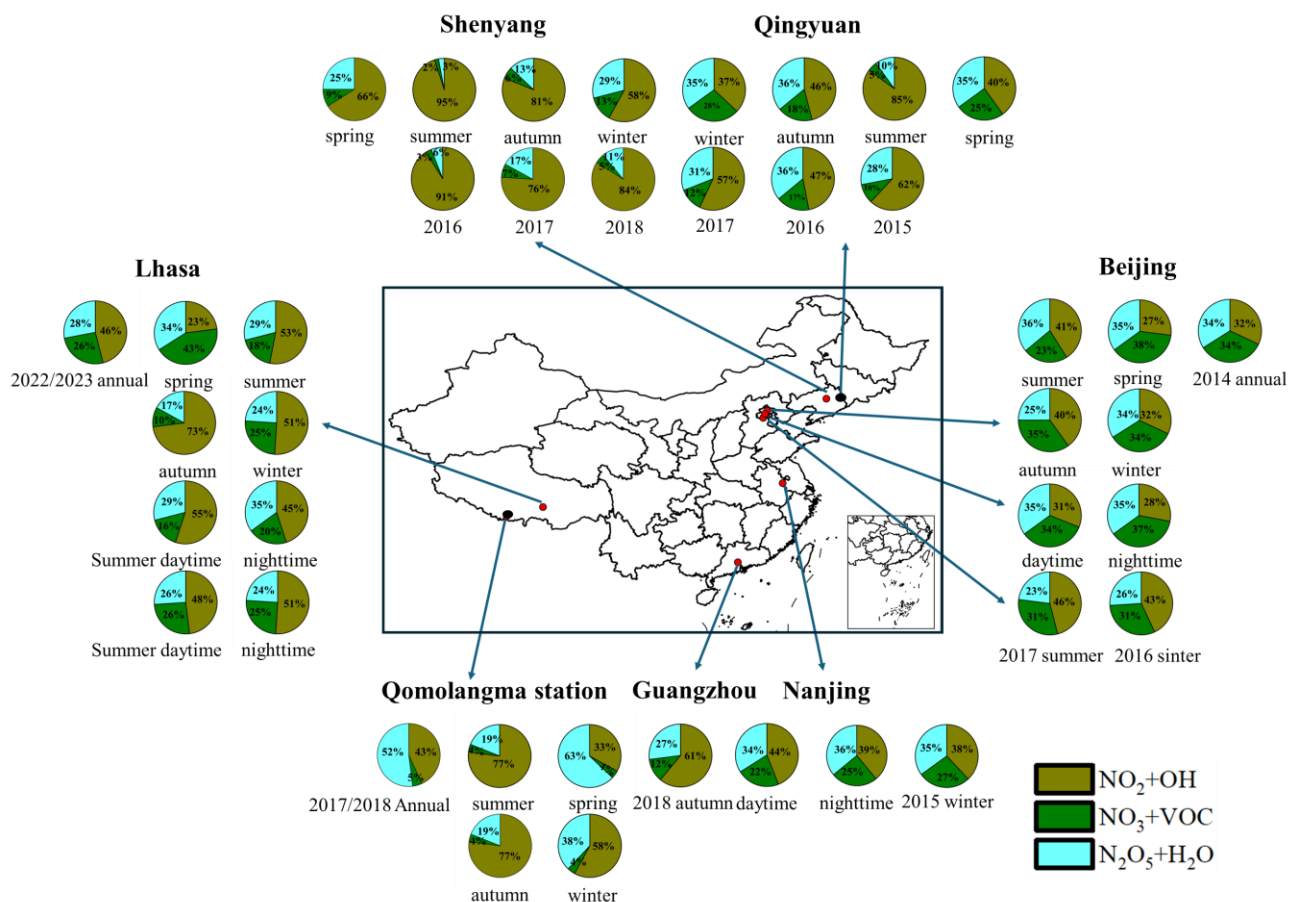


Figure 4. Summary of the relative contributions of key oxidation pathways using the  $\Delta^{17}\text{O}$  methodology around the China (data given in Table S4 in the Supplement). Colors for the study labels indicate the type of sampling location: urban areas (red), and rural/remote areas (black). The pie charts show the relative contribution of different pathways to  $\text{NO}_3^-$  formation:  $f_{\text{NO}_2+\text{OH}}$  ( deep yellow),  $f_{\text{NO}_3+\text{VOC}}$  deep green), and  $f_{\text{N}_2\text{O}_5+\text{H}_2\text{O}}$  (light blue).

## 4.2 Seasonal and diurnal variations of $\text{NO}_3^-$ oxidation pathways

Figure S7 illustrates the seasonal variations in the relative contributions of the three main oxidation pathways to  $\text{NO}_3^-$  formation. When comparing different seasons, the  $f_{\text{NO}_2+\text{OH}}$  values were lower ( $p < 0.01$ ) in spring (22.6%) than in winter (50.8%), summer (52.9%) and autumn (73.2%). The dominance of  $\text{NO}_2 + \text{OH}$  pathway in autumn is consistent with observations at Mt. Everest during the autumn seasons of 2017 and 2018, suggesting that  $\text{NO}_3^-$  formation on the Tibetan Plateau in autumn may be mainly driven by  $\text{NO}_2 + \text{OH}$  pathway (Lin et al., 2021; Wang et al., 2020b).

A significant increase in the  $f_{\text{NO}_3+\text{VOC}}$  values was observed in spring ( $p < 0.05$ ). First,  $\text{O}_3$  and  $\text{NO}_2$  are precursors of  $\text{NO}_3$ . In this work, the highest concentrations of  $\text{O}_3$  were found in spring ( $114.9 \pm 18.1 \mu\text{g}/\text{m}^3$ ), likely leading to elevated  $\text{NO}_3$  concentrations. Additionally, the low temperature and

reduced OH radical concentrations in spring facilitate the reaction of  $\text{NO}_2$  and  $\text{O}_3$  to synthesize  $\text{NO}_3$ . This might be an appropriate reason for the  $f_{\text{NO}_3+\text{VOC}}$  values in spring. High-altitude locations such as Nepal (5079 m a.s.l.) and Qomolangma Station (4300 m a.s.l.) have experienced stratospheric ozone intrusions, especially in spring and winter, as reported in previous studies (Zhang et al., 2025; Cristofanelli et al., 2010; Morin et al., 2007; Zhang et al., 2022; Lin et al., 2016; Yin et al., 2017; Wang et al., 2020b). Notably, such intrusions in spring may elevate tropospheric  $\text{O}_3$  levels in Lhasa, resulting in a mixture of tropospheric and stratospheric  $\text{O}_3$  that enhances  $\text{NO}_3^-$  production. Second, previous study has indicated that the Afghanistan-Pakistan-Tajikistan region, the Indo-Gangetic Plain, and Meghalaya-Myanmar region could transport industrial VOC to various zones in Tibet from west to east. Additionally, agricultural areas in northern India could contribute biomass burning-related VOC to the middle-northern and eastern regions of Tibet (Li et al., 2017). During our sampling campaign, South and Southeast Asia air clusters were notably prevalent in the springtime, coinciding with intensive fire spots observed in Afghanistan, Pakistan, India, Nepal, and Bhutan (Figure S3/S4). These observations, combined with the prevailing South and Southeast Asia air mass trajectories in spring, strongly suggest that long-range transported VOC from South Asia were delivered to Lhasa and likely participated in local  $\text{NO}_3^-$  production via  $\text{NO}_3 + \text{VOC}$  pathway. Moreover, recent studies have shown that ambient VOC concentrations in the urban areas on the Qinghai-Tibet Plateau were comparable to those in the North China Plain (Tang et al., 2022). The input of VOC through long-range transport might further elevate VOC concentrations, thereby promoting  $\text{NO}_3^-$  formation via  $\text{NO}_3 + \text{VOC}$  pathway and contributing to the enhanced  $f_{\text{NO}_3+\text{VOC}}$  values observed in spring. While VOC appears to play a dominant role in the process, it should be noted that other nitrogen species (e.g.,  $\text{NO}$ ,  $\text{NO}_2$ ) associated with biomass burning emissions may also be transported over long distances and influence  $\text{NO}_3^-$  formation in Lhasa. These co-transported nitrogen compounds, although not directly quantified in this study, could further contribute to  $\text{NO}_3^-$  production in spring. Taken together, these findings provide strong evidence that long-range transport of biomass burning emissions, particularly from South Asia, can substantially influence springtime  $\text{NO}_3^-$  formation in Lhasa.

Similarly, the  $f_{\text{N}_2\text{O}_5+\text{H}_2\text{O}}$  values exhibited its highest contributions during spring, with significant seasonal differences ( $p < 0.05$ ) except when compared to summer ( $p > 0.05$ ). Typically, high RH enhances  $\text{NO}_3^-$  formation via  $\text{N}_2\text{O}_5 + \text{H}_2\text{O}$  pathway. However, studies have revealed that during sandstorm events, a significant large  $\text{N}_2\text{O}_5$  uptake coefficient is observed on urban aerosols in spring

(Xia et al., 2019). In this study, the mean  $\text{Ca}^{2+}$  concentration in  $\text{PM}_{2.5}$  was found to be the highest in spring, suggesting a possible role of dust in facilitating  $\text{N}_2\text{O}_5$  uptake. Additionally,  $\text{N}_2\text{O}_5 + \text{H}_2\text{O}$  pathway has been reported to be promoted by elevated  $\text{NO}_3^-$  concentrations (Lin et al., 2021), which were also highest in spring. Therefore, the increased  $f_{\text{N}_2\text{O}_5+\text{H}_2\text{O}}$  values during spring might be attributed to the combined effects of lower RH, elevated  $\text{Ca}^{2+}$  levels, and high  $\text{NO}_3^-$  concentrations.

Interestingly, distinct diurnal patterns of  $\text{NO}_3^-$  oxidation pathways were observed during the sampling campaign (Figure 5). In summer,  $\text{NO}_2 + \text{OH}$  pathway showed a significantly higher contribution during the daytime (55.1%) compared to nighttime (44.9%), which is attributed to increased OH radical synthesis during longer days and higher temperatures in Lhasa (Rohrer and Berresheim, 2006). A previous study indicated that lower  $\text{NO}_2$  and higher  $\text{O}_3$  concentrations enhance the relative contribution of OH pathway to  $\text{NO}_3^-$  formation (Wang et al., 2019). Additionally, the concentration of ALWC (the detailed information is given in Text S3) was higher at night than during the day in summer, favoring  $\text{NO}_3^-$  formation through nocturnal formation. In winter,  $f_{\text{NO}_2+\text{OH}}$ ,  $f_{\text{NO}_3+\text{VOC}}$  and  $f_{\text{N}_2\text{O}_5+\text{H}_2\text{O}}$  were similar during both day and night. Typically, photolytic destruction and chemical reactions with NO are rapid sinks during the daytime, with lifetimes generally less than 5 seconds and resulting in extremely low concentrations. Similarly, the atmospheric lifetime of  $\text{N}_2\text{O}_5$  under sunlight is also very short (Wang et al., 2018). Thus, daytime  $\text{NO}_3$  and  $\text{N}_2\text{O}_5$  chemistry is often considered negligible. However, a recent study revealed that a non-negligible amount of  $\text{NO}_3$  radicals can persist during the daytime in cold months, owing to the limited solar radiation (Hellén et al., 2018). Wang et al. (2020a) found that the daytime production rate of  $\text{NO}_3$  can be substantial due to elevated concentrations of  $\text{O}_3$  and  $\text{NO}_2$ , suggesting that the mixing ratios of  $\text{NO}_3$  and  $\text{N}_2\text{O}_5$  during the day may not be negligible. Furthermore, in winter, lower temperatures and elevated  $\text{NO}_2$  concentrations facilitate a quasi-steady-state equilibrium between  $\text{NO}_3$  and  $\text{N}_2\text{O}_5$ , slowing the overall reactivity of the  $\text{NO}_3^-$  precursors (Brown et al., 2003). This equilibrium condition minimizes diurnal fluctuations in precursor concentrations, resulting in relatively stable nocturnal and daytime  $\text{NO}_3^-$  formation pathways, including  $\text{NO}_3 + \text{VOC}$  and  $\text{N}_2\text{O}_5 + \text{H}_2\text{O}$ . Nevertheless, we acknowledge that the exact role of daytime  $\text{NO}_3/\text{N}_2\text{O}_5$  chemistry remains uncertain in Lhasa and should be further assessed using concurrent field observations or chemical transport models. Moreover, when interpreting the diurnal differences in  $\Delta^{17}\text{O}-\text{NO}_3^-$  values, the atmospheric lifetime of  $\text{NO}_3^-$  must be considered. Given the atmospheric lifetime of  $\text{NO}_3^-$  is generally more than 12 hours, each sample might reflect both daytime and nighttime

NO<sub>3</sub><sup>-</sup> production impacting on Δ<sup>17</sup>O-NO<sub>3</sub><sup>-</sup> values (Park et al., 2004; Vicars et al., 2013).

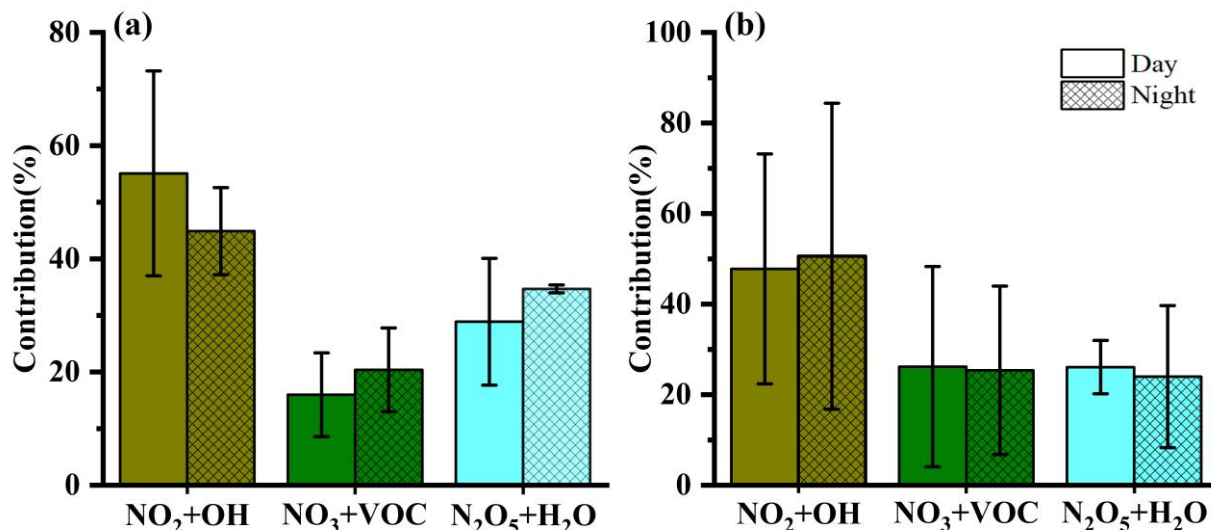


Figure 5. the relative contributions (mean ± SD values) of NO<sub>2</sub> + OH, NO<sub>3</sub> + VOC, and N<sub>2</sub>O<sub>5</sub> + H<sub>2</sub>O to NO<sub>3</sub><sup>-</sup> formation during the day and night (a) in summer and (b) winter in Lhasa during the sampling campaign.

### 4.3 Integrated analysis of NO<sub>3</sub><sup>-</sup> oxidation pathways in Lhasa

As shown in Figure S8, NO<sub>3</sub> + VOC pathway emerged as the major contributor to NO<sub>3</sub><sup>-</sup> formation during periods of high NO<sub>3</sub><sup>-</sup> spikes. To elucidate the NO<sub>3</sub><sup>-</sup> formation pathways under different NO<sub>3</sub><sup>-</sup> concentrations, NO<sub>3</sub><sup>-</sup> samples were categorized into different concentration ranges (Figure 6). We found the  $f_{\text{NO}_3+\text{VOC}}$  values increased and  $f_{\text{NO}_2+\text{OH}}$  values decreased with the NO<sub>3</sub><sup>-</sup> concentrations. Although recent field radical measurements in urban sites in China found that OH and HO<sub>2</sub> radical during haze period is comparable to clean days (Slater et al., 2020; Yang et al., 2021), our results suggested that NO<sub>3</sub>+VOC pathway still played an important role in NO<sub>3</sub><sup>-</sup> production under high-NO<sub>3</sub><sup>-</sup> concentration in Lhasa, possibly due to enhanced VOC emission. In addition to concentration effects, meteorological factors typically also regulate the NO<sub>3</sub><sup>-</sup> oxidation pathways. Typically, high temperature promotes the NO<sub>3</sub><sup>-</sup> formation in  $f_{\text{NO}_2+\text{OH}}$  values (Han et al., 2015). However, our study revealed that the relationship between temperature and  $f_{\text{NO}_2+\text{OH}}$  values did not consistently show a positive trend. Further analysis indicated that NO<sub>2</sub> and O<sub>3</sub> concentrations were negatively correlated, with lower NO<sub>2</sub> concentrations paired with elevated O<sub>3</sub> levels (Figure S9).  $f_{\text{NO}_2+\text{OH}}$  values reached its

460 minimum when  $\text{NO}_2$  was between 15 and 20  $\mu\text{g}/\text{m}^3$  and  $\text{O}_3$  was within 100-120  $\mu\text{g}/\text{m}^3$ . Although OH  
461 radicals exhibit a higher oxidation potential (2.8 V) than  $\text{O}_3$  (2.07 V), but atmospheric availability is  
462 much lower than that of  $\text{O}_3$  (Carslaw et al., 1999; Dubey et al., 1997). Therefore,  $\text{NO}_2$  at lower  
463 concentrations is more likely to be oxidized by OH than by  $\text{O}_3$ , even though  $\text{O}_3$  concentrations were  
464 high. With increasing  $\text{NO}_2$  concentrations, the availability of OH radicals for oxidating  $\text{NO}_2$  became  
465 lower, resulting in a relatively higher proportion of  $\text{NO}_2$  being oxidized by  $\text{O}_3$  although  $\text{O}_3$   
466 concentrations were low. However, when the concentration of  $\text{O}_3$  is below 20  $\mu\text{g}/\text{m}^3$ ,  $\text{O}_3$  concentrations  
467 were not sufficient to oxidize  $\text{NO}_2$  due to the higher  $\text{NO}_2$  concentrations and OH radicals for oxidating  
468  $\text{NO}_2$  would re-dominate. These observations underscore that in high-altitude urban environments like  
469 Lhasa, OH effectiveness is more important on  $\text{NO}_3^-$  oxidation pathways than that of  $\text{O}_3$ . Additionally,  
470 we identified an intriguing positive correlation between the atmospheric oxidizing capacity ( $\text{O}_x = \text{NO}_2$   
471 +  $\text{O}_3$ ) and  $f_{\text{NO}_3+\text{VOC}}$  values.  $f_{\text{NO}_3+\text{VOC}}$  values were lowest when  $\text{O}_x$  was less than 90  $\mu\text{g}/\text{m}^3$ , corresponding  
472 to a maximum contribution from the  $\text{NO}_2 + \text{OH}$  pathway. This suggests that  $\text{O}_x$  is more indicative of  
473 the pathways of  $\text{NO}_3^-$  formation in the atmosphere compared to either  $\text{NO}_2$  or  $\text{O}_3$  alone. Typically,  
474 High RH and ALWC were also positively correlated with  $f_{\text{N}_2\text{O}_5+\text{H}_2\text{O}}$ . But RH was associated with  
475 variable contributions from the  $\text{N}_2\text{O}_5+\text{H}_2\text{O}$  pathway in our study, while increasing ALWC significantly  
476 enhanced this pathway, indicating ALWC as a more reliable indicator of  $\text{NO}_3^-$  formation.

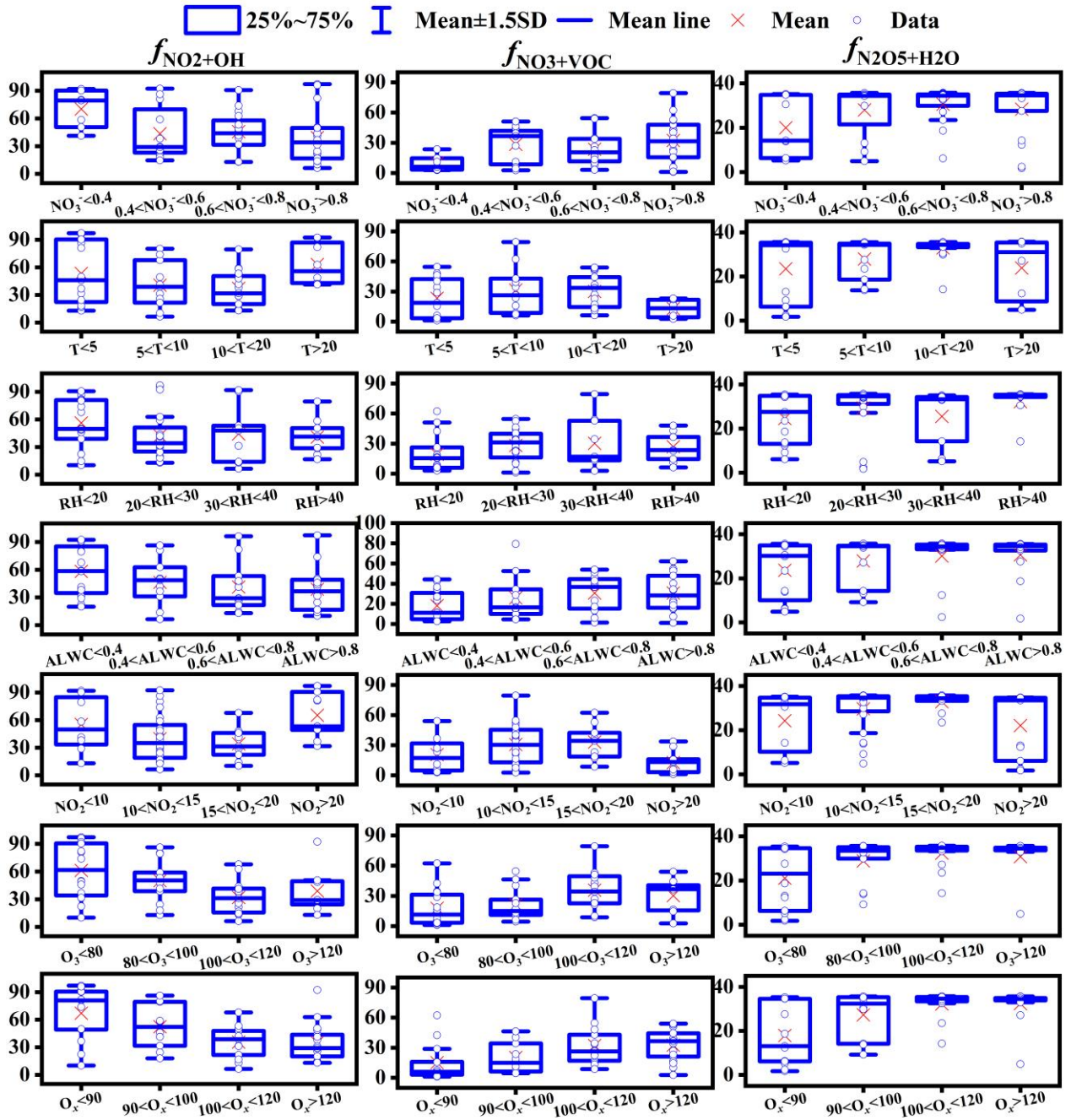


Figure 6 Influence of  $\text{NO}_3^-$  ( $\mu\text{g}/\text{m}^3$ ), temperature ( $^\circ\text{C}$ ), RH (%), ALWC ( $\mu\text{g}/\text{m}^3$ ),  $\text{NO}_2$  ( $\mu\text{g}/\text{m}^3$ ),  $\text{O}_3$  and  $\text{O}_x$  ( $\mu\text{g}/\text{m}^3$ ) on  $\text{NO}_3^-$  formation pathways (%).

#### 4.4 Implications

The oxidation pathways of  $\text{NO}_3^-$  in Lhasa, China, were constrained using a full year of  $\Delta^{17}\text{O}-\text{NO}_3^-$  measurements from 2022 to 2023. Based on seasonal data, we observed a significant increase in the relative contribution of the  $\text{NO}_3+\text{VOC}$  to  $\text{NO}_3^-$  formation during spring. Furthermore, the diurnal distribution of  $\text{NO}_3^-$  oxidation pathways varied distinctly across seasons. To better understand the factors influencing these pathways, we integrated meteorological conditions,  $\text{NO}_x$  precursors, and



ALWC for a more comprehensive analysis of  $\text{NO}_3^-$  formation. The results revealed that  $\text{O}_x$  and ALWC are more reliable indicators of  $\text{NO}_3^-$  oxidation pathways than meteorological factors. Notably, Lhasa's unique high-altitude environment such as strong solar radiation, persistently high  $\text{O}_3$ , and elevated VOC, promotes active  $\text{NO}_3 + \text{VOC}$  chemistry, especially in spring. Atmospheric ALWC is primarily produced by hygroscopic aerosols such as  $\text{SO}_4^{2-}$ ,  $\text{NH}_4^+$ , and  $\text{Cl}^-$ . Therefore, in addition to controlling  $\text{NO}_2$ ,  $\text{O}_3$ , and VOC, reducing these hygroscopic aerosols is crucial for effective  $\text{PM}_{2.5}$  pollution control.

Although this study provides valuable insights into  $\text{NO}_3^-$  formation mechanisms in Lhasa, we must acknowledge the associated uncertainties due to the lack of comprehensive observational constraints in Lhasa. Specifically, the limited understanding of local  $\text{RO}_2$  concentrations led us to adopt empirical parameterizations and refer to measurements from other regions, which inevitably introduce uncertainty into the pathway apportionment. In addition, the absence of direct observations of nighttime NO emissions and the  $\text{NO}_2$ -NO isotope exchange processes in this region further complicates the interpretation of diurnal variations in  $\text{NO}_3^-$  formation pathways. To improve the robustness of  $\Delta^{17}\text{O}$ -based pathway analysis, future studies should consider synchronous measurements of both  $\text{NO}_2$  and  $\text{NO}_3^-$  isotopes.

#### **Data availability**

All data are presented in the main text and/ or the Supplement. For additional data, please contact the corresponding author ([liu.junwen@jnu.edu.cn](mailto:liu.junwen@jnu.edu.cn)).

#### **Author contributors**

JL designed, conceived, and led the research. XZ performed the data analysis and drafted the manuscript. JL, XZ NC and BB planned and carried out the measurements. NC, BB and PD were responsible for measuring the meteorological parameters. JL and PY secured funding for the continuous aerosol sampling and analysis. FC and YZ provided expertise on isotope analysis methods. JL offered guidance on data analysis, and all authors contributed to revising the manuscript.

#### **Competing interests**

The authors declare no competing financial interest.

#### **Acknowledgments**

This study was supported by the Natural Science Foundation of Xizang Autonomous Region (XZ202401ZR0067), Guangdong Basic and Applied Basic Research Foundation (2024B1515040026),



516 the second Tibetan Plateau Scientific Expedition and Research Program (20190ZKK0604) and  
517 Guangdong Provincial General Colleges and Universities Innovation Team Project (Natural Science)  
518 (2024KCXTD004).  
519

## Reference

- Alexander, B., Hastings, M., Allman, D., Dachs, J., Thornton, J., and Kunasek, S.: Quantifying atmospheric nitrate formation pathways based on a global model of the oxygen isotopic composition ( $\Delta^{17}\text{O}$ ) of atmospheric nitrate, *Atmospheric Chemistry and Physics*, 9, 5043-5056, 2009.
- Alexander, B., Sherwen, T., Holmes, C. D., Fisher, J. A., Chen, Q., Evans, M. J., and Kasibhatla, P.: Global inorganic nitrate production mechanisms: comparison of a global model with nitrate isotope observations, *Atmospheric Chemistry and Physics*, 20, 3859-3877, 2020.
- Barkan, E. and Luz, B.: High-precision measurements of  $^{17}\text{O}/^{16}\text{O}$  and  $^{18}\text{O}/^{16}\text{O}$  of  $\text{O}_2$  and  $\text{O}_2/\text{Ar}$  ratio in air, *Rapid communications in mass spectrometry*, 17, 2809-2814, 2003.
- Bell, M. L., Dominici, F., Ebisu, K., Zeger, S. L., and Samet, J. M.: Spatial and temporal variation in  $\text{PM}_{2.5}$  chemical composition in the United States for health effects studies, *Environmental health perspectives*, 115, 989-995, 2007.
- Brown, S. S. and Stutz, J.: Nighttime radical observations and chemistry, *Chemical Society Reviews*, 41, 6405-6447, 2012.
- Brown, S. S., Stark, H., and Ravishankara, A.: Applicability of the steady state approximation to the interpretation of atmospheric observations of  $\text{NO}_3$  and  $\text{N}_2\text{O}_5$ , *Journal of Geophysical Research: Atmospheres*, 108, 2003.
- Cao, X., Xing, Q., Hu, S., Xu, W., Xie, R., Xian, A., Xie, W., Yang, Z., and Wu, X.: Characterization, reactivity, source apportionment, and potential source areas of ambient volatile organic compounds in a typical tropical city, *Journal of Environmental Sciences*, 123, 417-429, 2023.
- Carslaw, N., Creasey, D. J., Heard, D. E., Lewis, A. C., McQuaid, J. B., Pilling, M. J., Monks, P. S., Bandy, B. J., and Penkett, S. A.: Modeling OH,  $\text{HO}_2$ , and  $\text{RO}_2$  radicals in the marine boundary layer: 1. Model construction and comparison with field measurements, *Journal of Geophysical Research: Atmospheres*, 104, 30241-30255, <https://doi.org/10.1029/1999JD900783>, 1999.
- Chen, Z., Pei, C., Liu, J., Zhang, X., Ding, P., Dang, L., Zong, Z., Jiang, F., Wu, L., and Sun, X.: Non-agricultural source dominates the ammonium aerosol in the largest city of South China based on the vertical  $\delta^{15}\text{N}$  measurements, *Science of The Total Environment*, 848, 157750, 2022.
- Clark, C. M. and Tilman, D.: Loss of plant species after chronic low-level nitrogen deposition to prairie grasslands, *Nature*, 451, 712-715, 2008.
- Colmer, J., Hardman, I., Shimshack, J., and Voorheis, J.: Disparities in  $\text{PM}_{2.5}$  air pollution in the United

States, Science, 369, 575-578, 2020.

Cristofanelli, P., Bracci, A., Sprenger, M., Marinoni, A., Bonafè, U., Calzolari, F., Duchi, R., Laj, P., Pichon, J.-M., and Roccato, F.: Tropospheric ozone variations at the Nepal Climate Observatory-Pyramid (Himalayas, 5079 m asl) and influence of deep stratospheric intrusion events, *Atmospheric Chemistry and Physics*, 10, 6537-6549, 2010.

Daily, B., <https://xinwen.bjd.com.cn/content/s6340d130e4b0b60bbc5d4ecd.html>

Dubey, M. K., Mohrschladt, R., Donahue, N. M., and Anderson, J. G.: Isotope specific kinetics of hydroxyl radical (OH) with water (H<sub>2</sub>O): Testing models of reactivity and atmospheric fractionation, *The Journal of Physical Chemistry A*, 101, 1494-1500, 1997.

Espina-Martin, P., Perdrix, E., Alleman, L., and Coddeville, P.: Origins of the seasonal variability of PM<sub>2.5</sub> sources in a rural site in Northern France, *Atmospheric Environment*, 120660, 2024.

Fan, M.-Y., Zhang, Y.-L., Lin, Y.-C., Hong, Y., Zhao, Z.-Y., Xie, F., Du, W., Cao, F., Sun, Y., and Fu, P.: Important role of NO<sub>3</sub> radical to nitrate formation aloft in urban Beijing: Insights from triple oxygen isotopes measured at the tower, *Environmental Science & Technology*, 56, 6870-6879, 2021.

Feng, X., Chen, Y., Chen, S., Peng, Y., Liu, Z., Jiang, M., Feng, Y., Wang, L., Li, L., and Chen, J.: Dominant Contribution of NO<sub>3</sub> Radical to NO<sub>3</sub> Formation during Heavy Haze Episodes: Insights from High-Time Resolution of Dual Isotopes  $\Delta^{17}\text{O}$  and  $\delta^{18}\text{O}$ , *Environmental Science & Technology*, 57, 20726-20735, 2023.

Fisher, J. A., Jacob, D. J., Travis, K. R., Kim, P. S., Marais, E. A., Chan Miller, C., Yu, K., Zhu, L., Yantosca, R. M., Sulprizio, M. P., Mao, J., Wennberg, P. O., Crounse, J. D., Teng, A. P., Nguyen, T. B., St. Clair, J. M., Cohen, R. C., Romer, P., Nault, B. A., Wooldridge, P. J., Jimenez, J. L., Campuzano-Jost, P., Day, D. A., Hu, W., Shepson, P. B., Xiong, F., Blake, D. R., Goldstein, A. H., Misztal, P. K., Hanisco, T. F., Wolfe, G. M., Ryerson, T. B., Wisthaler, A., and Mikoviny, T.: Organic nitrate chemistry and its implications for nitrogen budgets in an isoprene- and monoterpene-rich atmosphere: constraints from aircraft (SEAC4RS) and ground-based (SOAS) observations in the Southeast US, *Atmos. Chem. Phys.*, 16, 5969-5991, 10.5194/acp-16-5969-2016, 2016.

Ge, S., Su, J., Zhao, P., Li, J., Liu, S., Qiu, Y., Pu, W., and Ma, Z.: Characteristics of PM<sub>2.5</sub> hygroscopicity and the influences of water-soluble ions during haze events in Beijing, *Atmospheric Environment*, 322, 120382, <https://doi.org/10.1016/j.atmosenv.2024.120382>, 2024.

Geng, G., Zheng, Y., Zhang, Q., Xue, T., Zhao, H., Tong, D., Zheng, B., Li, M., Liu, F., and Hong, C.:

580 Drivers of PM<sub>2.5</sub> air pollution deaths in China 2002–2017, *Nature Geoscience*, 14, 645–650, 2021.

581 Han, T., Liu, X., Zhang, Y., Qu, Y., Zeng, L., Hu, M., and Zhu, T.: Role of secondary aerosols in haze  
 582 formation in summer in the Megacity Beijing, *Journal of environmental sciences*, 31, 51–60, 2015.

583 He, P., Xie, Z., Chi, X., Yu, X., Fan, S., Kang, H., Liu, C., and Zhan, H.: Atmospheric  $\Delta^{17}\text{O}$  ( $\text{NO}_3^-$ )  
 584 reveals nocturnal chemistry dominates nitrate production in Beijing haze, *Atmospheric Chemistry  
 585 and Physics*, 18, 14465–14476, 2018.

586 He, S., Huang, M., Zheng, L., Chang, M., Chen, W., Xie, Q., and Wang, X.: Seasonal variation of  
 587 transport pathways and potential source areas at high inorganic nitrogen wet deposition sites in  
 588 southern China, *Journal of Environmental Sciences*, 114, 444–453,  
 589 <https://doi.org/10.1016/j.jes.2021.12.024>, 2022.

590 Hellén, H., Praplan, A. P., Tykkä, T., Ylivinkka, I., Vakkari, V., Bäck, J., Petäjä, T., Kulmala, M., and  
 591 Hakola, H.: Long-term measurements of volatile organic compounds highlight the importance of  
 592 sesquiterpenes for the atmospheric chemistry of a boreal forest, *Atmospheric Chemistry and Physics*,  
 593 18, 13839–13863, 2018.

594 Huang, R.-J., Zhang, Y., Bozzetti, C., Ho, K.-F., Cao, J.-J., Han, Y., Daellenbach, K. R., Slowik, J. G.,  
 595 Platt, S. M., and Canonaco, F.: High secondary aerosol contribution to particulate pollution during  
 596 haze events in China, *Nature*, 514, 218–222, 2014.

597 Ishino, S., Hattori, S., Savarino, J., Jourdain, B., Preunkert, S., Legrand, M., Caillon, N., Barbero, A.,  
 598 Kuribayashi, K., and Yoshida, N.: Seasonal variations of triple oxygen isotopic compositions of  
 599 atmospheric sulfate, nitrate, and ozone at Dumont d'Urville, coastal Antarctica, *Atmospheric  
 600 Chemistry and Physics*, 17, 3713–3727, 2017.

601 Kanaya, Y., Cao, R., Akimoto, H., Fukuda, M., Komazaki, Y., Yokouchi, Y., Koike, M., Tanimoto, H.,  
 602 Takegawa, N., and Kondo, Y.: Urban photochemistry in central Tokyo: 1. Observed and modeled  
 603 OH and HO<sub>2</sub> radical concentrations during the winter and summer of 2004, *Journal of Geophysical  
 604 Research: Atmospheres*, 112, 2007.

605 Kunasek, S., Alexander, B., Steig, E., Hastings, M., Gleason, D., and Jarvis, J.: Measurements and  
 606 modeling of  $\Delta^{17}\text{O}$  of nitrate in snowpits from Summit, Greenland, *Journal of Geophysical Research:  
 607 Atmospheres*, 113, 2008.

608 Lhasa, T. P. s. G. o., Overview of Lhasa: <https://www.lasa.gov.cn/lasa/yxls/yx.shtml>

609 Li, H., He, Q., Song, Q., Chen, L., Song, Y., Wang, Y., Lin, K., Xu, Z., and Shao, M.: Diagnosing

610 Tibetan pollutant sources via volatile organic compound observations, *Atmospheric Environment*,  
611 166, 244-254, 2017.

612 Li, Z., Walters, W. W., Hastings, M. G., Song, L., Huang, S., Zhu, F., Liu, D., Shi, G., Li, Y., and Fang,  
613 Y.: Atmospheric nitrate formation pathways in urban and rural atmosphere of Northeast China:  
614 Implications for complicated anthropogenic effects, *Environmental Pollution*, 296, 118752,  
615 <https://doi.org/10.1016/j.envpol.2021.118752>, 2022.

616 Lin, M., Zhang, Z., Su, L., Hill-Falkenthal, J., Priyadarshi, A., Zhang, Q., Zhang, G., Kang, S., Chan,  
617 C. Y., and Thiemens, M. H.: Resolving the impact of stratosphere-to-troposphere transport on the  
618 sulfur cycle and surface ozone over the Tibetan Plateau using a cosmogenic  $^{35}\text{S}$  tracer, *Journal of*  
619 *Geophysical Research: Atmospheres*, 121, 439-456, 2016.

620 Lin, Y.-C., Zhang, Y.-L., Yu, M., Fan, M.-Y., Xie, F., Zhang, W.-Q., Wu, G., Cong, Z., and Michalski,  
621 G.: Formation mechanisms and source apportionments of airborne nitrate aerosols at a Himalayan-  
622 Tibetan Plateau site: Insights from nitrogen and oxygen isotopic compositions, *Environmental*  
623 *Science & Technology*, 55, 12261-12271, 2021.

624 Luo, L., Kao, S., Wu, Y., Zhang, X., Lin, H., Zhang, R., and Xiao, H.: Stable oxygen isotope constraints  
625 on nitrate formation in Beijing in springtime, *Environmental Pollution*, 263, 114515, 2020.

626 Michalski, G., Scott, Z., Kabling, M., and Thiemens, M. H.: First measurements and modeling of  
627  $\Delta^{17}\text{O}$  in atmospheric nitrate, *Geophysical Research Letters*, 30, 2003.

628 Morin, S., Savarino, J., Bekki, S., Gong, S., and Bottenheim, J.: Signature of Arctic surface ozone  
629 depletion events in the isotope anomaly ( $\Delta^{17}\text{O}$ ) of atmospheric nitrate, *Atmospheric Chemistry and*  
630 *Physics*, 7, 1451-1469, 2007.

631 Park, R. J., Jacob, D. J., Field, B. D., Yantosca, R. M., and Chin, M.: Natural and transboundary  
632 pollution influences on sulfate-nitrate-ammonium aerosols in the United States: Implications for  
633 policy, *Journal of Geophysical Research: Atmospheres*, 109, 2004.

634 Parnell, A. C., Inger, R., Bearhop, S., and Jackson, A. L.: Source partitioning using stable isotopes:  
635 coping with too much variation, *PloS one*, 5, e9672, 2010.

636 Qiu, X., Ying, Q., Wang, S., Duan, L., Zhao, J., Xing, J., Ding, D., Sun, Y., Liu, B., Shi, A., Yan, X.,  
637 Xu, Q., and Hao, J.: Modeling the impact of heterogeneous reactions of chlorine on summertime  
638 nitrate formation in Beijing, China, *Atmos. Chem. Phys.*, 19, 6737-6747, 10.5194/acp-19-6737-  
639 2019, 2019.

640 Rohrer, F. and Berresheim, H.: Strong correlation between levels of tropospheric hydroxyl radicals and  
641 solar ultraviolet radiation, *Nature*, 442, 184-187, 2006.

642 Salameh, D., Detournay, A., Pey, J., Pérez, N., Liguori, F., Saraga, D., Bove, M. C., Brotto, P., Cassola,  
643 F., and Massabò, D.: PM<sub>2.5</sub> chemical composition in five European Mediterranean cities: A 1-year  
644 study, *Atmospheric Research*, 155, 102-117, 2015.

645 Savarino, J., Vicars, W. C., Legrand, M., Preunkert, S., Jourdain, B., Frey, M. M., Kukui, A., Caillon,  
646 N., and Gil Roca, J.: Oxygen isotope mass balance of atmospheric nitrate at Dome C, East Antarctica,  
647 during the OPAL campaign, *Atmospheric Chemistry and Physics*, 16, 2659-2673, 2016.

648 Slater, E. J., Whalley, L. K., Woodward-Massey, R., Ye, C., Lee, J. D., Squires, F., Hopkins, J. R.,  
649 Dunmore, R. E., Shaw, M., Hamilton, J. F., Lewis, A. C., Crilley, L. R., Kramer, L., Bloss, W., Vu,  
650 T., Sun, Y., Xu, W., Yue, S., Ren, L., Acton, W. J. F., Hewitt, C. N., Wang, X., Fu, P., and Heard, D.  
651 E.: Elevated levels of OH observed in haze events during wintertime in central Beijing, *Atmos.*  
652 *Chem. Phys.*, 20, 14847-14871, 10.5194/acp-20-14847-2020, 2020.

653 Song, W., Wang, Y.-L., Yang, W., Sun, X.-C., Tong, Y.-D., Wang, X.-M., Liu, C.-Q., Bai, Z.-P., and  
654 Liu, X.-Y.: Isotopic evaluation on relative contributions of major NO<sub>x</sub> sources to nitrate of PM<sub>2.5</sub> in  
655 Beijing, *Environmental Pollution*, 248, 183-190, 2019.

656 Su, X., Tie, X., Li, G., Cao, J., Huang, R., Feng, T., Long, X., and Xu, R.: Effect of hydrolysis of N<sub>2</sub>O<sub>5</sub>  
657 on nitrate and ammonium formation in Beijing China: WRF-Chem model simulation, *Science of*  
658 *The Total Environment*, 579, 221-229, <https://doi.org/10.1016/j.scitotenv.2016.11.125>, 2017.

659 Sun, P., Farley, R. N., Li, L., Srivastava, D., Niedek, C. R., Li, J., Wang, N., Cappa, C. D., Pusede, S.  
660 E., and Yu, Z.: PM<sub>2.5</sub> composition and sources in the San Joaquin Valley of California: A long-term  
661 study using ToF-ACSM with the capture vaporizer, *Environmental Pollution*, 292, 118254, 2022.

662 Tang, G., Yao, D., Kang, Y., Liu, Y., Liu, Y., Wang, Y., Bai, Z., Sun, J., Cong, Z., Xin, J., Liu, Z., Zhu,  
663 Z., Geng, Y., Wang, L., Li, T., Li, X., Bian, J., and Wang, Y.: The urgent need to control volatile  
664 organic compound pollution over the Qinghai-Tibet Plateau, *iScience*, 25, 105688,  
665 <https://doi.org/10.1016/j.isci.2022.105688>, 2022.

666 Vicars, W., Morin, S., Savarino, J., Wagner, N., Erbland, J., Vince, E., Martins, J., Lerner, B., Quinn,  
667 P., and Coffman, D.: Spatial and diurnal variability in reactive nitrogen oxide chemistry as reflected  
668 in the isotopic composition of atmospheric nitrate: Results from the CalNex 2010 field study, *Journal*  
669 *of Geophysical Research: Atmospheres*, 118, 10,567-510,588, 2013.

670 Vicars, W. C. and Savarino, J.: Quantitative constraints on the  $^{17}\text{O}$ -excess ( $\Delta^{17}\text{O}$ ) signature of surface  
671 ozone: Ambient measurements from 50 N to 50 S using the nitrite-coated filter technique,  
672 *Geochimica et Cosmochimica Acta*, 135, 270-287, 2014.

673 Vicars, W. C., Bhattacharya, S., Erbland, J., and Savarino, J.: Measurement of the  $^{17}\text{O}$ -excess ( $\Delta^{17}\text{O}$ )  
674 of tropospheric ozone using a nitrite-coated filter, *Rapid Communications in Mass Spectrometry*,  
675 26, 1219-1231, 2012.

676 Walters, W. W., Pye, H. O., Kim, H., and Hastings, M. G.: Modeling the Oxygen Isotope Anomaly  
677 ( $\Delta^{17}\text{O}$ ) of Reactive Nitrogen in the Community Multiscale Air Quality Model: Insights into Nitrogen  
678 Oxide Chemistry in the Northeastern United States, *ACS ES&T Air*, 2024.

679 Wang, H., Chen, X., Lu, K., Hu, R., Li, Z., Wang, H., Ma, X., Yang, X., Chen, S., Dong, H., Liu, Y.,  
680 Fang, X., Zeng, L., Hu, M., and Zhang, Y.:  $\text{NO}_3$  and  $\text{N}_2\text{O}_5$  chemistry at a suburban site during the  
681 EXPLORE-YRD campaign in 2018, *Atmospheric Environment*, 224, 117180,  
682 <https://doi.org/10.1016/j.atmosenv.2019.117180>, 2020a.

683 Wang, H., Lu, K., Guo, S., Wu, Z., Shang, D., Tan, Z., Wang, Y., Le Breton, M., Lou, S., Tang, M.,  
684 Wu, Y., Zhu, W., Zheng, J., Zeng, L., Hallquist, M., Hu, M., and Zhang, Y.: Efficient  $\text{N}_2\text{O}_5$  uptake  
685 and  $\text{NO}_3$  oxidation in the outflow of urban Beijing, *Atmos. Chem. Phys.*, 18, 9705-9721,  
686 10.5194/acp-18-9705-2018, 2018.

687 Wang, K., Hattori, S., Kang, S., Lin, M., and Yoshida, N.: Isotopic constraints on the formation  
688 pathways and sources of atmospheric nitrate in the Mt. Everest region, *Environmental Pollution*,  
689 267, 115274, 2020b.

690 Wang, Y., Liu, J., Jiang, F., Chen, Z., Wu, L., Zhou, S., Pei, C., Kuang, Y., Cao, F., and Zhang, Y.:  
691 Vertical measurements of stable nitrogen and oxygen isotope composition of fine particulate nitrate  
692 aerosol in Guangzhou city: Source apportionment and oxidation pathway, *Science of The Total  
693 Environment*, 865, 161239, 2023.

694 Wang, Y. L., Song, W., Yang, W., Sun, X. C., Tong, Y. D., Wang, X. M., Liu, C. Q., Bai, Z. P., and Liu,  
695 X. Y.: Influences of atmospheric pollution on the contributions of major oxidation pathways to  $\text{PM}_{2.5}$   
696 nitrate formation in Beijing, *Journal of Geophysical Research: Atmospheres*, 124, 4174-4185, 2019.

697 Xia, M., Wang, W., Wang, Z., Gao, J., Li, H., Liang, Y., Yu, C., Zhang, Y., Wang, P., Zhang, Y., Bi, F.,  
698 Cheng, X., and Wang, T.: Heterogeneous Uptake of  $\text{N}_2\text{O}_5$  in Sand Dust and Urban Aerosols  
699 Observed during the Dry Season in Beijing, *Atmosphere*, 10, 204, 2019.

- Xu, Q., Wang, S., Jiang, J., Bhattarai, N., Li, X., Chang, X., Qiu, X., Zheng, M., Hua, Y., and Hao, J.: Nitrate dominates the chemical composition of PM<sub>2.5</sub> during haze event in Beijing, China, *Science of the Total Environment*, 689, 1293-1303, 2019.
- Yang, X., Lu, K., Ma, X., Liu, Y., Wang, H., Hu, R., Li, X., Lou, S., Chen, S., and Dong, H.: Observations and modeling of OH and HO<sub>2</sub> radicals in Chengdu, China in summer 2019, *Science of The Total Environment*, 772, 144829, 2021.
- Yin, M., Guan, H., Luo, L., Xiao, H., and Zhang, Z.: Using nitrogen and oxygen stable isotopes to analyze the major NO<sub>x</sub> sources to nitrate of PM<sub>2.5</sub> in Lanzhou, northwest China, in winter-spring periods, *Atmospheric Environment*, 276, 119036, 2022.
- Yin, X., Kang, S., de Foy, B., Cong, Z., Luo, J., Zhang, L., Ma, Y., Zhang, G., Rupakheti, D., and Zhang, Q.: Surface ozone at Nam Co in the inland Tibetan Plateau: variation, synthesis comparison and regional representativeness, *Atmospheric Chemistry and Physics*, 17, 11293-11311, 2017.
- Zhang, Q., Zheng, Y., Tong, D., Shao, M., Wang, S., Zhang, Y., Xu, X., Wang, J., He, H., and Liu, W.: Drivers of improved PM<sub>2.5</sub> air quality in China from 2013 to 2017, *Proceedings of the National Academy of Sciences*, 116, 24463-24469, 2019.
- Zhang, Q., Jiang, X., Tong, D., Davis, S. J., Zhao, H., Geng, G., Feng, T., Zheng, B., Lu, Z., Streets, D. G., Ni, R., Brauer, M., van Donkelaar, A., Martin, R. V., Huo, H., Liu, Z., Pan, D., Kan, H., Yan, Y., Lin, J., He, K., and Guan, D.: Transboundary health impacts of transported global air pollution and international trade, *Nature*, 543, 705-709, 10.1038/nature21712, 2017.
- Zhang, Y.-L., Zhang, W., Fan, M.-Y., Li, J., Fang, H., Cao, F., Lin, Y.-C., Wilkins, B. P., Liu, X., and Bao, M.: A diurnal story of  $\Delta^{17}\text{O}(\text{NO}_3^-)$  in urban Nanjing and its implication for nitrate aerosol formation, *npj Climate and Atmospheric Science*, 5, 50, 2022.
- Zhang, Y., Zhao, T., Ning, G., Xu, X., Chen, Z., Jia, M., Sun, X., Shu, Z., Lu, Z., and Liu, J.: A unique mechanism of ozone surges jointly triggered by deep stratospheric intrusions and the Tibetan Plateau topographic forcing, *Geophysical Research Letters*, 52, e2024GL114207, 2025.
- Zhang, Z., Jiang, Z., Zhou, T., and Geng, L.: Reconciling Modeled and Observed  $\Delta^{17}\text{O}(\text{NO}_3^-)$  in Beijing Winter Haze With Heterogeneous Chlorine Chemistry, *Journal of Geophysical Research: Atmospheres*, 129, e2023JD039740, <https://doi.org/10.1029/2023JD039740>, 2024.
- Zhao, M., Huang, Z., Qiao, T., Zhang, Y., Xiu, G., and Yu, J.: Chemical characterization, the transport pathways and potential sources of PM<sub>2.5</sub> in Shanghai: Seasonal variations, *Atmospheric Research*,



730 158, 66-78, 2015.

731 Zong, Z., Tan, Y., Wang, X., Tian, C., Li, J., Fang, Y., Chen, Y., Cui, S., and Zhang, G.: Dual-modelling-

732 based source apportionment of NO<sub>x</sub> in five Chinese megacities: Providing the isotopic footprint

733 from 2013 to 2014, *Environment International*, 137, 105592,

734 <https://doi.org/10.1016/j.envint.2020.105592>, 2020.

735